Instabilities in the free inflation of a nonlinear hyperelastic toroidal membrane

Sairam Pamulaparthi Venkata[a,b], Prashant Saxena[b,c*]

[a]Department of Mechanical and Aerospace Engineering, Field of Theoretical and Applied Mechanics, Cornell University, Ithaca, NY 14853, USA

[b]Department of Mechanical & Aerospace Engineering, Indian Institute of Technology Hyderabad, Kandi, Sangareddy 502285, Telangana, India

[c]Glasgow Centre for Computational Engineering, James Watt School of Engineering University of Glasgow, Rankine Building, Glasgow G12 8LT, UK

Abstract

Study on an incompressible nonlinear hyperelastic thin-walled toroidal membrane of circular cross-section subjected to inflation due to a uniform pressure is conducted in this work. Comparisons are made for three elastic constitutive models (neo-Hookean, Mooney–Rivlin, and Ogden) and for different geometric aspect ratios (ratio of the radius of cross-section to the radius of revolution). A variational approach is used to derive the equations of equilibrium and bifurcation. An analysis of the pressure–deformation plots shows occurrence of the well-known limit point (snap through) instabilities in membrane. Calculations are performed to study the elastic buckling point to predict bifurcation of solution corresponding to loss of symmetry. Tension field theory is employed to study the wrinkling instability that, in this case, typically occurs near the inner regions of tori with large aspect ratios.

Keywords: membrane; limit point; wrinkling; bifurcation; nonlinear elasticity; finite deformation

MSC2010 classification: 74B20, 74G60, 74K15

Note: This is author-generated version of the article published in the Journal of Mechanics of Materials and Structures (2019).

*Corresponding author, Email: prashant.saxena@glasgow.ac.uk

Contents

1 Introduction

Nonlinear elastic membranes are widely used to make engineering structures and occur naturally as biological tissues. Air bags, diaphragm valves, balloons, and soft tissues like skin, arterial walls and cell walls are some examples of this structure category. Large deformation due to inflation in membranes is typically associated with several instability modes and the behaviour strongly depends on the geometric and material nonlinearities. In this work, we study the inflation of an incompressible toroidal membrane under hydrostatic pressure and the instabilities accompanying the large deformation. We present new results and analyses for different constitutive models, limit points, buckling, and wrinkling instabilities in this, otherwise, extensively studied problem.

Axisymmetric deformations of toroidal membranes have been studied for several decades, for example, see the early works of Clark (1950), Jordan (1962), and Liepins and

Sanders (1963). By using perturbation technique, an approximate solution for a thick-walled toroidal membrane made of neo-Hookean material is given by Kydoniefs and Spencer (1965) and for a thin-walled toroidal membrane by Kydoniefs and Spencer (1967). Yang and Feng (1970) examined the problems concerning large axisymmetric deformations of nonlinear membranes of Mooney–Rivlin type by employing standard numerical techniques. Hill (1980) determined analytical solutions for a thick-walled toroidal membrane using the Mooney–Rivlin model. Asymptotic behaviour of a nonlinear torus was studied by Bonadies (1987) using an assumption that overall radius of the torus is large in comparison to the radius of larger circle generating the torus. Application of finite-element formulation to numerically analyse axisymmetric incompressible nonlinear elastic membranes of general shape which exhibit finite strains can be found in the works of Wriggers and Taylor (1990), Gruttmann and Taylor (1992), and Başar and Itskov (1998). Numerical studies by Holzapfel et al. (1996) and Humphrey (1998) shine light on remarkable success of finite-element approach to understand axisymmetric nonlinear behaviour of anisotropic biomembranes and cells under finite strain. Xin-chun and Chang-jun (1991) employed Runge-Kutta numerical method followed by Newton-Raphson iterative technique to study axisymmetric deformation of hyperelastic toroidal membrane with finite strains by considering volume of the gas inside the torus (monotonic function) as a control parameter instead of internal pressure (non-monotonic function). Papargyri-Pegiou (1995) examined a pressurised compressible thin-walled nonlinear toroidal membrane by comparing the stability of analytical solution obtained from perturbation approach with the numerical results. Papargyri-Pegiou and Stavrakakis (2000) applied a numerical scheme to study an incompressible thin-walled nonlinear torus under internal pressure for different elastic constitutive models. Papargyri-Beskou (2005) developed a finite-element method to numerically determine stresses and deformations in both compressible and incompressible thin-walled toroidal membrane under static inflation using Levenberg-Marquardt algorithm. By varying the geometric and material parameters, Tamadapu and DasGupta (2012) studied in-plane deformations in homogeneous inflated elastic toroidal membranes made of neo-Hookean and Mooney–Rivlin materials using discretization methods for both isotropic and anisotropic cases. A direct integration method coupled with Nelder-Mead optimisation technique was formulated to determine numerical solutions for toroidal membranes by Tamadapu and DasGupta (2014) and Roychowdhury and DasGupta (2015).

Typical deformation characteristics of membranes under inflation involve the phenomenon of limit point or snap through instability. A peak pressure is reached for a given deformation beyond which the membrane inflates rapidly with the slightest increase in pressure. These instabilities have been widely studied for membranes of various shapes by Benedict et al. (1979), Dreyer et al. (1982), Carroll (1987), Khayat et al. (1992), and Müller and Struchtrup (2002). Kanner and Horgan (2007) investigated the effect of strain-hardening on limit point instability in thin-walled spherical and cylindrical shells for different constitutive models and material parameters. Tamadapu et al. (2013) analysed the effects of geometric and material parameters on limit point pressure and the associated instabilities during inflation of incompressible nonlinear elastic membranes of Mooney–Rivlin type, including the torus. Reddy and Saxena (2017, 2018) employed

both analytical and numerical schemes to study limit point instability in toroidal and cylindrical magnetoelastic membranes. Application of bifurcation theory to study buckling problems in the case of a general elastic deformation is a well-developed research area, see, for example the classical works of Koiter (1945) and Budiansky (1974).

During the process of stretching, a local structural instability in the form of wrinkling is typically observed in thin-walled elastic membranes for certain geometries and material parameters (Harold and Grenville, 1970, Szyszkowski and Glockner, 1987, Jenkins et al., 1998). Due to unequal stretching in the principal directions during inflation, compressive stresses may develop in certain regions of the membrane causing out of plane displacements. According to the tension field theory (Pipkin, 1986), the wrinkles orient along the direction of the positive principal stress and the wrinkling occurs in the direction of negative principal stress. The component of principal stress along the direction of wrinkling is considered to be zero by Pipkin (1986). Steigmann (1990) extended this theory to nonlinear elastic membranes and developed analytical functions to obtain information about stretch and the alignment of tension lines in membranes undergoing wrinkling. It is to be noted that, as no bending stiffness is assigned to the membrane, the amplitude and wavelength of the wrinkles cannot be computed by using this theory. Research on the wrinkling of membranes include those by Stein and Hedgepeth (1961), Wu (1974, 1978), Wu and Canfield (1981), Mansfield (1981), Zak (1982), Haughton and McKay (1995), Epstein (1999), Saxena et al. (2019), to name a few. Axisymmetric deformations of tense and wrinkled zones in thin-walled elastic isotropic membranes were found by Li and Steigmann (1995a,b) using relaxed form of Ogden's three terms strain energy model, by Roxburgh (1995) using relaxed form of Mooney–Rivlin strain energy function, and by Steigmann (2005) using relaxed form of Varga strain energy function. Wong and Pellegrino (2006) proposed an analytical method to determine the location of wrinkles and quantify the geometrical patterns such as amplitude and wavelength in linear elastic membranes. Nayyar et al. (2011) and Barsotti (2015) applied finite-element methods to study wrinkling in thin-walled elastic membranes. Patil et al. (2015) used a combination of standard and relaxed strain energy density functions to numerically determine the nonlinear axisymmetric deformations in tensed and wrinkled regions for an incompressible cylindrical membrane with non-uniform thickness. The numerical analysis was performed by applying finite difference method coupled with the Newton-Raphson iterative technique.

In this work, we analyse the influence of geometry and material parameters on axisymmetric deformations, limit points, bifurcation points, and wrinkling of inflated isotropic hyperelastic toroidal membrane under a uniform hydrostatic pressure. The two-point boundary value problem obtained from the equilibrium equations is converted into an initial value problem. Then, for a given deformation of a point on the outer equator of the membrane, shooting method is employed to capture the unknown initial conditions using Nelder–Mead optimisation technique and coupled with a direct integration method to solve the resulting equilibrium equations. We apply the classical theory of instability developed by Koiter (1945) and Budiansky (1974) by considering pressure as the loading parameter to compute the bifurcation point at which the symmetric fundamental solution

becomes unstable. It is observed that bifurcation for torus of neo-Hookean type typically occurs very close to the limit point for the first mode except for the smallest aspect ratio case in which it occurs post limit point for the second mode. Location of wrinkled region is computed using an iterative process based on a kinematic condition that helps in an accurate recomputation of the entire solution using a coupled form of standard and relaxed energy to determine the membrane deformation.

Remainder of this paper is organised as follows. In Section 2, we formulate the problem statement along with the necessary kinematical equations for the reference and deformed configurations of the toroidal membrane. In Section 3, we formulate the governing equations of elastic equilibrium using the first variation of the total potential energy functional. We introduce three different elastic constitutive models (Ogden, Mooney–Rivlin, and neo-Hookean) used for computations and also derive the governing equations corresponding to wrinkling by using relaxed strain energy density. In Section 4, second variation of the strain-energy functional is derived for the neo-Hookean model to compute critical pressure for buckling. We discuss the numerical procedure used for computations and present our results and analysis in Section 5. Finally, we present the conclusions in Section 6.

2 Kinematics of deformation

Consider the reference and deformed configurations of an isotropic incompressible hyperelastic thin-walled toroidal membrane of a circular cross-section as shown in Figure 1. Smaller radius is R_s and the radius of revolution is R_b in the reference configuration. The toroidal membrane is inflated by an internal hydrostatic pressure. Thickness of the undeformed and deformed membranes are denoted by T and t, respectively related by the stretch ratio $\lambda_3 = t/T$. Thinness assumption requires $T \ll R_s$. Profile of the mid-surface of torus in the deformed configuration can be traced using two functions $\widetilde{\varrho}$ and $\widetilde{\eta}$ as shown in the figure. The torus is symmetric about the $Y^1 - Y^2$ plane, hence we constrain the solution space and study only the deformations of the toroidal membrane with respect to the upper half of the $Y^1 - Y^2$ plane. The calculations and notation below closely follow those in (Reddy and Saxena, 2017).

It can be shown that the covariant metric tensors G_{ij} and $\widetilde{g}_{ij}$ in the reference and deformed configurations, respectively, are given by

$$[G_{ij}] = \begin{bmatrix} R_s^2 & 0 & 0 \\ 0 & R_b^2 R^2 & 0 \\ 0 & 0 & 1 \end{bmatrix}, \qquad [\widetilde{g}_{ij}] = \begin{bmatrix} \widetilde{\varrho}_\theta^2 + \widetilde{\eta}_\theta^2 & \widetilde{\varrho}_\theta \widetilde{\varrho}_\phi + \widetilde{\eta}_\theta \widetilde{\eta}_\phi & 0 \\ \widetilde{\varrho}_\theta \widetilde{\varrho}_\phi + \widetilde{\eta}_\theta \widetilde{\eta}_\phi & \widetilde{\varrho}_\phi^2 + \widetilde{\varrho}^2 + \widetilde{\eta}_\phi^2 & 0 \\ 0 & 0 & \lambda_3^2 \end{bmatrix}, \tag{1}$$

where $R = \left[1 + \frac{R_s}{R_b} \cos\theta\right]$, and a subscript with respect to θ or ϕ denote a partial derivative, i.e. $(\bullet)_\theta = \partial(\bullet)/\partial\theta$, $(\bullet)_\phi = \partial(\bullet)/\partial\phi$.

Upon introducing the non-dimensional parameters

$$\gamma = \frac{R_s}{R_b}, \quad \varrho = \frac{\widetilde{\varrho}}{R_b}, \quad \eta = \frac{\widetilde{\eta}}{R_b}, \tag{2}$$

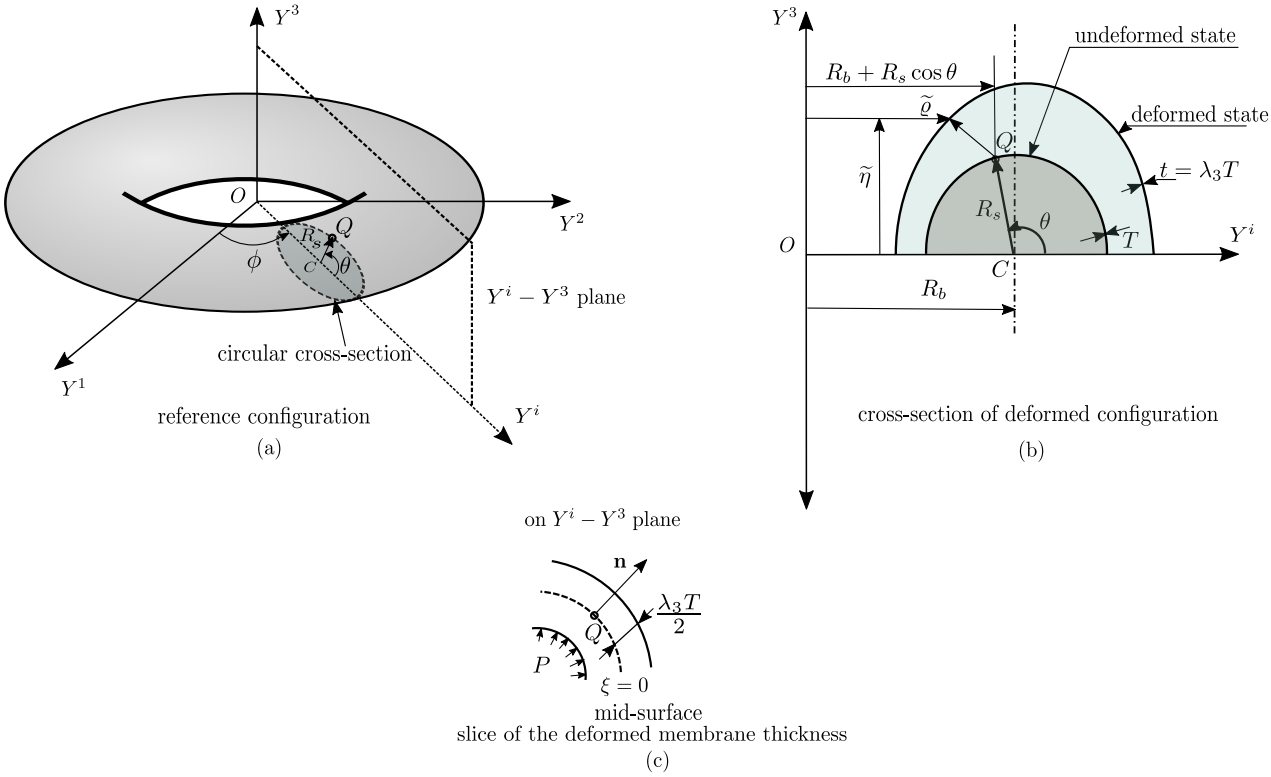

Figure 1: Toroidal membrane (a) before deformation with a circular cross-section highlighted, (b) the cross-section after general deformation illustrated through a point Q on $Y^i - Y^3$ plane, and (c) a slice of the membrane thickness acted upon by an internal pressure P. The membrane at any instant is symmetric about $Y^1 - Y^2$ plane and about the Y^3 axis.

and applying the constraint of incompressibility $\det(\mathbf{F}) = 1$, $\mathbf{F}$ being the deformation gradient tensor, we can write the principal stretch ratios $\lambda_1, \lambda_2, \lambda_3$ as

$$\begin{aligned}
\lambda_1^2 &= \frac{1}{2}\left[\frac{\varrho_\theta^2+\eta_\theta^2}{\gamma^2}+\frac{\varrho_\phi^2+\eta_\phi^2+\varrho^2}{R^2}\right]+\frac{1}{2}\sqrt{\left[\frac{\varrho_\theta^2+\eta_\theta^2}{\gamma^2}-\frac{\varrho_\phi^2+\eta_\phi^2+\varrho^2}{R^2}\right]^2+4\left[\frac{\varrho_\theta\varrho_\phi+\eta_\theta\eta_\phi}{\gamma R}\right]^2} \\
\lambda_2^2 &= \frac{1}{2}\left[\frac{\varrho_\theta^2+\eta_\theta^2}{\gamma^2}+\frac{\varrho_\phi^2+\eta_\phi^2+\varrho^2}{R^2}\right]-\frac{1}{2}\sqrt{\left[\frac{\varrho_\theta^2+\eta_\theta^2}{\gamma^2}-\frac{\varrho_\phi^2+\eta_\phi^2+\varrho^2}{R^2}\right]^2+4\left[\frac{\varrho_\theta\varrho_\phi+\eta_\theta\eta_\phi}{\gamma R}\right]^2} \\
\lambda_3^2 &= \frac{1}{\lambda_1^2\lambda_2^2} = \frac{\gamma^2R^2}{\left[\left[\varrho_\theta^2+\eta_\theta^2\right]\left[\varrho_\phi^2+\eta_\phi^2+\varrho^2\right]-\left[\varrho_\theta\varrho_\phi+\eta_\theta\eta_\phi\right]^2\right]} = \frac{\gamma^2R^2}{\left[\varrho_\theta\eta_\phi-\varrho_\phi\eta_\theta\right]^2+\varrho^2\left[\varrho_\theta^2+\eta_\theta^2\right]}.
\end{aligned} \tag{3}$$

3 Energy considerations and governing equations

3.1 Potential energy and equilibrium equations

The total potential energy functional E of the system of interest is given by

$$E\left[\varrho,\eta\right] = T\int_\Omega W dA - \int_{V_0}^{V_0+\Delta V}\widetilde{P}dV, \tag{4}$$

where T is the thickness of undeformed membrane, Ω represents the mid-surface of the undeformed membrane, V_0 represents the enclosed initial volume and ΔV measures the change in the enclosed volume, $W\left(\varrho,\varrho_\theta,\varrho_\phi,\eta_\theta,\eta_\phi\right)$ is the strain energy per unit undeformed volume, and $\widetilde{P}$ is the hydrostatic pressure. Note that W has no explicit dependence on η since none of the principal stretch ratios depend on η as seen from equations (3).

Equation (4) can be rewritten as

$$E\left[\varrho,\eta\right] = T\int_0^{2\pi}\int_0^{2\pi} W\sqrt{G}d\theta d\phi - \int_0^{2\pi}\int_0^{2\pi}\widetilde{P}\mathbf{n}da\cdot\delta\mathbf{y}, \tag{5}$$

where $\sqrt{G} = \sqrt{\det\left(G_{ij}\right)} = RR_sR_b$ and $da = \sqrt{g}d\theta d\phi$ is the area of a differential element on the deformed surface with the unit normal $\mathbf{n}$. Note that the strain energy is calculated over the reference configuration while the pressure work is evaluated over the deformed configuration.

First variation of the total potential energy is given as

$$\begin{aligned}
\delta E = T\int_0^{2\pi}\int_0^{2\pi}&\left[\left[\frac{\partial W}{\partial\varrho}\sqrt{G}-\frac{\partial}{\partial\theta}\left(\frac{\partial W}{\partial\varrho_\theta}\sqrt{G}\right)-\frac{\partial}{\partial\phi}\left(\frac{\partial W}{\partial\varrho_\phi}\sqrt{G}\right)\right]\delta\varrho\right. \\
&\left.-\left[\frac{\partial}{\partial\theta}\left(\frac{\partial W}{\partial\eta_\theta}\sqrt{G}\right)+\frac{\partial}{\partial\phi}\left(\frac{\partial W}{\partial\eta_\phi}\sqrt{G}\right)\right]\delta\eta\right]d\theta d\phi \\
&+\int_0^{2\pi}\int_0^{2\pi}\widetilde{P}R_b^3\Big[\left[\varrho\varrho_\theta\right]\delta\eta-\left[\varrho\eta_\theta\right]\delta\varrho\Big]d\theta d\phi.
\end{aligned} \tag{6}$$

From the principle of minimum potential energy, equilibrium states are attained when $\delta E = 0$ that results in the following Euler equations to be satisfied for evaluating the principal solution of deformation

$$\frac{\partial}{\partial\theta}\left(\frac{\partial W}{\partial \varrho_\theta}\sqrt{G}\right) + \frac{\partial}{\partial\phi}\left(\frac{\partial W}{\partial \varrho_\phi}\sqrt{G}\right) - \frac{\partial W}{\partial \varrho}\sqrt{G} + \frac{\widetilde{P}R_b^3}{T}\left[\varrho\eta_\theta\right] = 0, \tag{7a}$$

$$\frac{\partial}{\partial\theta}\left(\frac{\partial W}{\partial \eta_\theta}\sqrt{G}\right) + \frac{\partial}{\partial\phi}\left(\frac{\partial W}{\partial \eta_\phi}\sqrt{G}\right) - \frac{\widetilde{P}R_b^3}{T}\left[\varrho\varrho_\theta\right] = 0. \tag{7b}$$

The fundamental solution is symmetric with respect to rotation about the Y^3 axis resulting in $\varrho_\phi = \eta_\phi = 0$. Upon using this condition, equation (7a) is simplified to

$$\frac{\partial^2 W}{\partial\theta\partial\varrho_\theta}\gamma R - \frac{\partial W}{\partial\varrho_\theta}\gamma^2\sin\theta - \frac{\partial W}{\partial\varrho}\gamma R + \frac{\widetilde{P}R_b}{T}\varrho\eta_\theta = 0, \tag{8}$$

and equation (7b) becomes

$$\frac{\partial^2 W}{\partial\theta\partial\eta_\theta}\gamma R - \frac{\partial W}{\partial\eta_\theta}\gamma^2\sin\theta - \frac{\widetilde{P}R_b}{T}\varrho\varrho_\theta = 0. \tag{9}$$

The governing equations (8) and (9) are solved using the boundary conditions which are determined based on compatibility and symmetry of the cross-section of the torus

$$\varrho_\theta(0) = \varrho_\theta(\pi) = 0, \qquad \eta(0) = \eta(\pi) = 0. \tag{10}$$

3.1.1 Elastic constitutive models

In order to demonstrate mechanical behaviour via computations we use the three-term Ogden, Mooney–Rivlin, and neo-Hookean hyperelastic models for the elastic strain energy density W in this work. These are three very commonly used hyperelastic energy density functions in several computational studies (Holzapfel, 2000). The mathematical expressions and numerical values of the material parameters are given below.

The strain energy density for the three-term Ogden model is given by

$$W^*(\lambda_1,\lambda_2) = \sum_{j=1}^{3}\frac{\mu_j}{\alpha_j}\left[\lambda_1^{\alpha_j} + \lambda_2^{\alpha_j} + \left[\frac{1}{\lambda_1\lambda_2}\right]^{\alpha_j} - 3\right], \tag{11}$$

along with the conditions $\sum_j \mu_j\alpha_j = 2\mu$ and $\mu_j\alpha_j > 0$. The non-dimensional parameters can be defined as $\mu_1^* = \frac{\mu_1}{\mu}, \mu_2^* = \frac{\mu_2}{\mu}, \mu_3^* = \frac{\mu_2}{\mu}$, μ being the baseline shear modulus.

Upon substituting $\alpha_1 = 2$, $\alpha_2 = -2$, and $\mu_3 = 0$ in equation (11), we arrive at the Mooney–Rivlin strain energy density given by

$$W^*(\lambda_1,\lambda_2) = \frac{\mu_1}{2}\left[\lambda_1^2 + \lambda_2^2 + \frac{1}{\lambda_1^2\lambda_2^2} - 3\right] - \frac{\mu_2}{2}\left[\frac{1}{\lambda_1^2} + \frac{1}{\lambda_2^2} + \lambda_1^2\lambda_2^2 - 3\right]. \tag{12}$$

Upon using $\alpha_1 = 2, \mu_2 = \mu_3 = 0$ in equation (11), we arrive at the neo-Hookean strain energy density given by

$$W^*(\lambda_1,\lambda_2) = \frac{\mu_1}{2}\left[\lambda_1^2 + \lambda_2^2 + \frac{1}{\lambda_1^2\lambda_2^2} - 3\right]. \tag{13}$$

Upon substitution of the explicit expressions of each of the above energy density functions, the resulting governing equations (8) and (9) can be rewritten as a system of first order ODEs in matrix form as below

$$\begin{bmatrix} 1 & 0 & 0 & 0 \\ 0 & \mathcal{S}_{22} & 0 & \mathcal{S}_{24} \\ 0 & 0 & 1 & 0 \\ 0 & \mathcal{S}_{42} & 0 & \mathcal{S}_{44} \end{bmatrix} \begin{bmatrix} \mathcal{U}_1' \\ \mathcal{U}_2' \\ \mathcal{U}_3' \\ \mathcal{U}_4' \end{bmatrix} = \begin{bmatrix} \mathcal{U}_2 \\ \mathcal{V}_1 \\ \mathcal{U}_4 \\ \mathcal{V}_2 \end{bmatrix}, \tag{14}$$

where

$$\mathcal{U}_1 = \varrho, \quad \mathcal{U}_2 = \varrho_\theta = \mathcal{U}_1', \quad \mathcal{U}_2' = \varrho_{\theta\theta}, \quad \mathcal{U}_3 = \eta, \quad \mathcal{U}_4 = \eta_\theta = \mathcal{U}_3', \quad \mathcal{U}_4' = \eta_{\theta\theta}, \tag{15}$$

and the remaining terms $S_{22}, S_{24}, S_{42}, S_{44}, \mathcal{V}_1, \mathcal{V}_2$ for each of the constitutive models are listed in Appendix A.1–A.3.

3.2 Relaxed strain energy density

During the inflation of elastic membranes, compressive stresses might develop for certain geometries as the membrane undergoes unequal stretching in the principal directions. As membranes are no-compression structures, these in-plane negative stresses result in out of plane deformations causing wrinkling instability. According to the Tension field theory, with the absence of bending stiffness in thin membranes, infinitesimally small and closely spaced wrinkles are formed due to compressive stresses. We observe the compressive stresses for certain geometries and for specific material parameters in our study. Pipkin (1986) proposed the concept of 'relaxed strain energy density' by modifying the elastic constitutive relation based on principal stretches to study the wrinkling behaviour in linear elastic membranes. This theory is extended to nonlinear elastic membranes by Steigmann (1990). The relaxed strain energy density, W_R is represented as

$$W_R = \begin{cases} W(\lambda_1, \lambda_2) & \text{if } \lambda_2 \geq w(\lambda_1) \text{ and } \lambda_1 \geq w(\lambda_2), \\ W_t(\lambda_1) & \text{if } \lambda_2 \leq w(\lambda_1) \text{ and } \lambda_1 \geq 1, \\ W_t(\lambda_2) & \text{if } \lambda_1 \leq w(\lambda_2) \text{ and } \lambda_2 \geq 1, \\ 0 & \text{if } \lambda_1 \leq 1 \text{ and } \lambda_2 \leq 1. \end{cases} \tag{16}$$

where the function $w(\lambda)$ is termed as the 'natural width in simple tension' and defined below. For any fixed value of λ_1, the minimum of W with respect to λ_2 is attained at

$$\lambda_2 = \lambda_1^{-\frac{1}{2}} =: w(\lambda_1). \tag{17}$$

Similarly, for any fixed value of λ_2, the minimum of W with respect to λ_1 is attained at

$$\lambda_1 = \lambda_2^{-\frac{1}{2}} = w(\lambda_2). \tag{18}$$

As compressive stresses develop in the region $\lambda_1 \geq 1$ and $\lambda_2 \leq w(\lambda_1)$, we can replace the original strain energy density function W by $W_t(\lambda_1)$ as mentioned in equation (16).

The terms $S_{22}, S_{24}, S_{42}, S_{44}, \mathcal{V}_1, \mathcal{V}_2$ in the governing equation (14) for computations in the wrinkled region should be modified according to the above-stated conditions and are given in Appendix A.4.

4 Second variation of total potential energy functional

In elastic solids, we often observe critical (buckling) points for certain load values at which the equilibrium path branches out into multiple stable and/or unstable paths. These critical points are of considerable interest as the post-buckling response of the system is usually different from the initial response (principal solution). Considering the hydrostatic pressure as a loading parameter, we adopt the procedure proposed by Budiansky (1974) to determine the critical pressure in our case of hyperelastic membrane beyond which the symmetric fundamental solution is no longer the energy minimizer. To reduce the complexity of long mathematical expressions, we study the critical pressure condition only for the neo-Hookean material model.

4.1 Critical pressure

The fundamental solution for ϱ and η is symmetric with respect to the Y^3 axis and therefore has no dependence on ϕ. We define critical pressure as the point where the solution loses this symmetry while retaining the symmetry with respect to the $Y^1 - Y^2$ plane. Hence, we consider the bifurcation branches that include perturbations in the ϕ direction. The following expansions are considered for the variables ϱ and η

$$\begin{aligned}
\varrho(\theta,\phi) &= \varrho_0(\theta) + \widehat{\varrho}(\phi) = \varrho_0(\theta) + \Upsilon\varrho_1(\phi) + \cdots, \\
\eta(\theta,\phi) &= \eta_0(\theta) + \widehat{\eta}(\phi) = \eta_0(\theta) + \Upsilon\eta_1(\phi) + \cdots, \\
\Upsilon &= \langle\widehat{\varrho}, \varrho_1\rangle = \langle\widehat{\eta}, \eta_1\rangle, \\
\langle\varrho_i, \varrho_j\rangle &= \langle\eta_i, \eta_j\rangle = \begin{cases} 1 & \text{if } i = j, \\ 0 & \text{otherwise} \end{cases},
\end{aligned} \tag{19}$$

where the scalar parameter $\Upsilon \ll 1$ measures the amount of bifurcation mode, $\langle\cdot\rangle$ represents a suitable inner product, and ϱ_1 and η_1 represent the first bifurcation mode with ϱ_0 and η_0 being the fundamental states.
Bifurcation of the solution occurs when the second variation of the potential energy vanishes. For the current scenario, it is given as

$$\begin{aligned}
\delta^2 E = E_c'' U_1 \delta U = &\left[E''_{c_{\alpha_1}} + E''_{c_{\alpha_2}} - E''_{c_{\alpha_{31}}} - E''_{c_{\alpha_{32}}} + E''_{c_{\alpha_{33}}} + E''_{c_{\alpha_{34}}}\right] U_1\delta U \\
&+ \left[-E''_{c_{\alpha_{35}}} + E''_{c_{\alpha_{36}}} + E''_{c_P}\right] U_1\delta U = 0,
\end{aligned} \tag{20}$$

where we have defined several terms as below

$$E''_{c_{\alpha_1}} U_1\delta U = 0, \tag{21}$$

$$E''_{c_{\alpha_2}} U_1\delta U = 2\bar{\mu}T \int_0^{2\pi}\int_0^{2\pi} \frac{\varrho_{1_\phi}\delta\varrho_\phi + \eta_{1_\phi}\delta\eta_\phi + \varrho_1\delta\varrho}{R^2}\sqrt{G}d\theta d\phi, \tag{22}$$

$$E''_{c_{\alpha_{31}}} U_1\delta U = 2\bar{\mu}T\gamma^2 \int_0^{2\pi}\int_0^{2\pi} \frac{\mathcal{E}_{aa}\mathcal{E}_{ab}}{\mathcal{E}_{ac}^2}\sqrt{G}R^2 d\theta d\phi, \tag{23}$$

$$E''_{c_{\alpha_{32}}} U_1 \delta U = 2\bar{\mu} T \gamma^2 \int_0^{2\pi} \int_0^{2\pi} \frac{\left[\varrho_\theta \eta_\phi - \varrho_\phi \eta_\theta\right] \left[\eta_{1_\phi} \delta\varrho_\theta - \varrho_{1_\phi} \delta\eta_\theta\right]}{\mathcal{E}_{ac}^2} \sqrt{G} R^2 d\theta d\phi, \tag{24}$$

$$E''_{c_{\alpha_{33}}} U_1 \delta U = 8\bar{\mu} T \gamma^2 \int_0^{2\pi} \int_0^{2\pi} \frac{\left[\varrho_\theta \eta_\phi - \varrho_\phi \eta_\theta\right]^2 \mathcal{E}_{aa} \mathcal{E}_{ab}}{\mathcal{E}_{ac}^3} \sqrt{G} R^2 d\theta d\phi, \tag{25}$$

$$E''_{c_{\alpha_{34}}} U_1 \delta U = 8\bar{\mu} T \gamma^2 \int_0^{2\pi} \int_0^{2\pi} \frac{\Big[\varrho_\theta \eta_\phi - \varrho_\phi \eta_\theta\Big] \mathcal{E}_{ad} \mathcal{E}_{ab}}{\mathcal{E}_{ac}^3} \sqrt{G} R^2 d\theta d\phi, \tag{26}$$

$$E''_{c_{\alpha_{35}}} U_1 \delta U = 2\bar{\mu} T \gamma^2 \int_0^{2\pi} \int_0^{2\pi} \frac{\varrho_1 \left[\varrho_\theta^2 + \eta_\theta^2\right] \delta\varrho + 2\varrho\varrho_1 \left[\varrho_\theta \delta\varrho_\theta + \eta_\theta \delta\eta_\theta\right]}{\mathcal{E}_{ac}^2} \sqrt{G} R^2 d\theta d\phi, \tag{27}$$

$$E''_{c_{\alpha_{36}}} U_1 \delta U = 8\bar{\mu} T \gamma^2 \int_0^{2\pi} \int_0^{2\pi} \frac{\varrho\varrho_1 \Big[\varrho_\theta^2 + \eta_\theta^2\Big] \Big[\big[\varrho_\theta \eta_\phi - \varrho_\phi \eta_\theta\big] \mathcal{E}_{aa} + \mathcal{E}_{ad}\Big]}{\mathcal{E}_{ac}^3} \sqrt{G} R^2 d\theta d\phi, \tag{28}$$

$$E''_{c_P} U_1 \delta U = \int_0^{2\pi} \int_0^{2\pi} \widetilde{P} R_b^3 \left[\varrho_\theta \eta_1 \delta\varrho + \varrho \eta_1 \delta\varrho_\theta - \eta_\theta \varrho_1 \delta\varrho - \varrho\varrho_1 \delta\eta_\theta\right] d\theta d\phi, \tag{29}$$

with

$$\mathcal{E}_{aa} = \eta_\phi \delta\varrho_\theta + \varrho_\theta \delta\eta_\phi - \eta_\theta \delta\varrho_\phi - \varrho_\phi \delta\eta_\theta, \quad \mathcal{E}_{ab} = \varrho_\theta \eta_{1_\phi} - \eta_\theta \varrho_{1_\phi}, \quad \bar{\mu} = \frac{\mu_1}{2},$$
$$\mathcal{E}_{ac} = \big[\varrho_\theta \eta_\phi - \varrho_\phi \eta_\theta\big]^2 + \varrho^2 \big[\varrho_\theta^2 + \eta_\theta^2\big], \quad \mathcal{E}_{ad} = \varrho \big[\varrho_\theta^2 + \eta_\theta^2\big] \delta\varrho + \varrho^2 \big[\varrho_\theta \delta\varrho_\theta + \eta_\theta \delta\eta_\theta\big]. \tag{30}$$

Upon separating the coefficients of $\delta\varrho$ and $\delta\eta$, we obtain the following governing equations for the bifurcated mode

$$\mathcal{K}_{aa} \varrho_1 + \mathcal{K}_{bb} \varrho_{1_{\phi\phi}} + \mathcal{K}_{cc} \eta_{1_{\phi\phi}} = 0, \tag{31}$$

and

$$\mathcal{L}_{aa} \varrho_1 + \mathcal{L}_{bb} \varrho_{1_{\phi\phi}} + \mathcal{L}_{cc} \eta_{1_{\phi\phi}} = 0, \tag{32}$$

where the bifurcation pressure is denoted as $\widetilde{P}_c$ and

$$\begin{aligned}
\mathcal{K}_{aa} &= R\gamma\varrho^4 \mathcal{N}^3 + 3R^5\gamma^3 \mathcal{N}^2 + 6\varrho_\theta^2 R^5 \gamma^3 \mathcal{N} - 2\varrho\varrho_{\theta\theta} R^5 \gamma^3 \mathcal{N} + 6\varrho\varrho_\theta R^4 \gamma^4 \mathcal{N} \sin\theta \\
&\quad + 8\varrho\varrho_\theta \left[\varrho_\theta \varrho_{\theta\theta} + \eta_\theta \eta_{\theta\theta}\right] R^5 \gamma^3 - \frac{P_c \eta_\theta}{2} R^2 \varrho^4 \mathcal{N}^3, \\
\mathcal{K}_{bb} &= -\varrho^4 \gamma R \mathcal{N}^3 + \eta_\theta^2 R^5 \gamma^3 \mathcal{N}, \quad \mathcal{K}_{cc} = -\varrho_\theta \eta_\theta R^5 \gamma^3 \mathcal{N}, \\
\mathcal{N} &= \varrho_\theta^2 + \eta_\theta^2, \quad P_c = \frac{\widetilde{P}_c R_b}{\bar{\mu} T}, \\
\mathcal{L}_{aa} &= 6\varrho_\theta \eta_\theta R^5 \gamma^3 \mathcal{N} - 2\varrho \eta_{\theta\theta} R^5 \gamma^3 \mathcal{N} + 6\varrho \eta_\theta R^4 \gamma^4 \mathcal{N} \sin\theta + 8\varrho\eta_\theta \left[\varrho_\theta \varrho_{\theta\theta} + \eta_\theta \eta_{\theta\theta}\right] R^5 \gamma^3 \\
&\quad + \frac{P_c}{2} \varrho^4 \varrho_\theta R^2 \mathcal{N}^3, \quad \mathcal{L}_{bb} = -\varrho_\theta \eta_\theta R^5 \mathcal{N} \gamma^3, \quad \mathcal{L}_{cc} = -\gamma R \varrho^4 \mathcal{N}^3 + \varrho_\theta^2 R^5 \gamma^3 \mathcal{N}.
\end{aligned} \tag{33}$$

Upon considering the following ansatz for ϱ_1 and η_1

$$\varrho_1 = \varrho_1^0 \exp(in\phi), \quad \eta_1 = \eta_1^0 \exp(in\phi), \qquad \text{where} \quad i = \sqrt{-1}, \tag{34}$$

it can be shown that a non-trivial solution for the above system of equation exists when

$$\mathcal{R}_{\text{res}} = \Big[\big[\mathcal{K}_{cc}\mathcal{L}_{aa} - \mathcal{K}_{aa}\mathcal{L}_{cc}\big] + n^2 \big[\mathcal{K}_{bb}\mathcal{L}_{cc} - \mathcal{K}_{cc}\mathcal{L}_{bb}\big]\Big] = 0. \tag{35}$$

The residue $\mathcal{R}_{\text{res}}$ defined above should be put to zero computationally in order to calculate the critical pressure value.

5 Numerical procedure, results, and discussion

Computations are performed for numerical values of the material parameters presented in Table 1.

Table 1: Non-dimensional material parameters used for numerical computations.

Three-term Ogden model (Ogden, 1972)					
$\mu_1^* = 1.4910$	$\mu_2^* = 0.0029$	$\mu_3^* = -0.0236$	$\alpha_1 = 1.3$	$\alpha_2 = 5.0$	$\alpha_3 = -2.0$
Mooney-Rivlin model			$\mathfrak{M} = -\frac{\mu_2}{\mu_1} = 0.1$ and 0.3		

5.1 Calculation of fundamental solution

The governing equations (8) and (9) for fundamental solution are subjected to boundary conditions defined by equation (10). They are numerically solved for three elastic constitutive models (Ogden, Mooney–Rivlin, and neo-Hookean) by following a method used for similar problems by Tamadapu and DasGupta (2014) and Reddy and Saxena (2017). The two point boundary value problem is converted into an initial value problem with two unknown parameters $(\varrho(0), \eta_\theta(0))$ at a particular non-dimensional pressure P. For a given value of location of point on the outer equator of the membrane $(\varrho(0) > 1+\gamma)$, we start with an initial guess for the pair $(\eta_\theta(0), P)$, and employ shooting method to obtain the two boundary values $\varrho_\theta(\pi)$ and $\eta(\pi)$ for the point on the inner edge. Ideally $\varrho_\theta(\pi)$ and $\eta(\pi)$ should be zero. The desired optimisation pair $(\eta_\theta(0), P)$ which reduces the value of the cost function, $\left[\varrho_\theta(\pi)^2 + \eta(\pi)^2\right]^{\frac{1}{2}}$, to a sufficiently small quantity $(< \mathcal{O}(10^{-12}))$ is obtained by using the Nelder-Mead simplex optimisation technique of two variables. This optimisation method is performed using fminsearchbnd function with lower bounds on the guess pair $(\{\eta_\theta(0), P\} > 0)$ in Matlab R2017b. As we capture the desired pair, we use a strong mass-state dependent ode45 solver in Matlab R2017b to solve the set of equilibrium equations in order to obtain the values of $\varrho, \varrho_\theta, \eta, \eta_\theta$ over the domain $\theta \in [0, \pi]$ which is finely divided into 2000 intervals.

5.1.1 Fundamental solution, deformation profiles, and validation

We plot the inflation profiles of the toroidal membrane for the Ogden model in Figure 2 for the aspect ratios $\gamma = 0.2$ and $\gamma = 0.7$. Similar profiles are obtained for all the models, aspect ratios, and pressure values but not shown here for brevity. It can be seen from Figure 2a that for the small aspect ratio ($\gamma = 0.2$), both the inner and the outer ends move outwards while for higher aspect ratio ($\gamma = 0.7$) and Figure 2b, inner end remains at almost the same position while the outer end moves outwards upon the increase of pressure.

Plots of $\varrho(\pi)$ (inner end) vs $\varrho(0)$ (outer end) for all the three material models and several aspect ratios $\{\gamma \in (0.2, 0.7)$ for Ogden and Mooney–Rivlin, $\gamma \in (0.2, 0.8)$ for neo-Hookean$\}$ are presented in Figure 3. For the Ogden and neo-Hookean models, it is clearly seen that upon the increase of inflation (moving rightwards on the $\varrho(0)$ axis), the inner end first moves slightly inwards and then moves outwards for almost all values of γ. Only for large aspect ratios ($\gamma = 0.7$ for Ogden and $\gamma = 0.7, 0.8$ for neo-Hookean), the inner

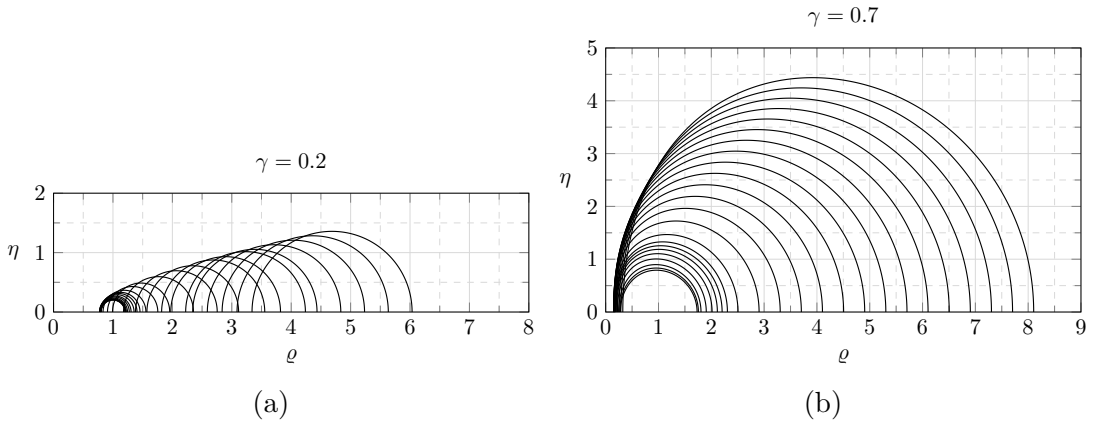

(a) (b)

Figure 2: Deformation profiles of the membrane subject to inflation using Ogden energy density function for aspect ratios $\gamma = 0.2$ and $\gamma = 0.7$. The non-dimensional coordinates ϱ and η are introduced in equation (2). Due to symmetry, only the upper half is plotted.

end undergoes very small changes in its position. This is also expected physically since tori with large γ have very little room for movement of the inner end. The behaviour is different for the two Mooney–Rivlin material models as shown in Figure 3c and Figure 3d. For the cases $\{\gamma = 0.2 \text{ to } 0.5, \mathfrak{M} = 0.1\}$ and $\{\gamma = 0.2, \mathfrak{M} = 0.3\}$, with an increase in pressure the inner edge moves outwards before moving inwards again for higher inflation. For all other cases, the inner edge moves further inwards monotonically upon increase of pressure.

These considerable differences in behaviours of constitutive models demonstrate the importance of selecting the right model for the material at hand. For example, behaviour of natural rubbers can usually be explained by the three-term Ogden model (Ogden, 1972) while that of certain soft biological tissues can be simulated by the neo-Hookean model (Horný et al., 2007). Our results for the Mooney–Rivlin model match those presented by Tamadapu and DasGupta (2014) for $\mathfrak{M} = 0.3, \gamma = 0.2$ and 0.5 cases, and those presented by Reddy and Saxena (2017) for $\mathfrak{M} = 0.1, \gamma = 0.2$ and 0.5; thus providing a validation of the formulation and the computations.

5.1.2 Limit point and Cauchy stress

We compute the pressure-deformation and pressure-stress characteristics for all the three material models for the aspect ratios lying in the range $\gamma \in (0.2, 0.8)$. Variation of non-dimensional pressure (P) with the relative increase in volume ($\Delta V/V$) of torus for three representative aspect ratios $\gamma = 0.2, 0.4$, and 0.6 is shown in Figure 4. In each of these curves we observe the classical limit point as the point at which pressure stops increasing monotonically. In a pressure controlled experiment, this generally results in a snap-through instability causing uncontrolled increase in membrane's volume likely leading to failure. However, the states beyond limit point can be reached in a volume controlled experiment.

It is evident from these curves that tori with small aspect ratios γ can sustain much

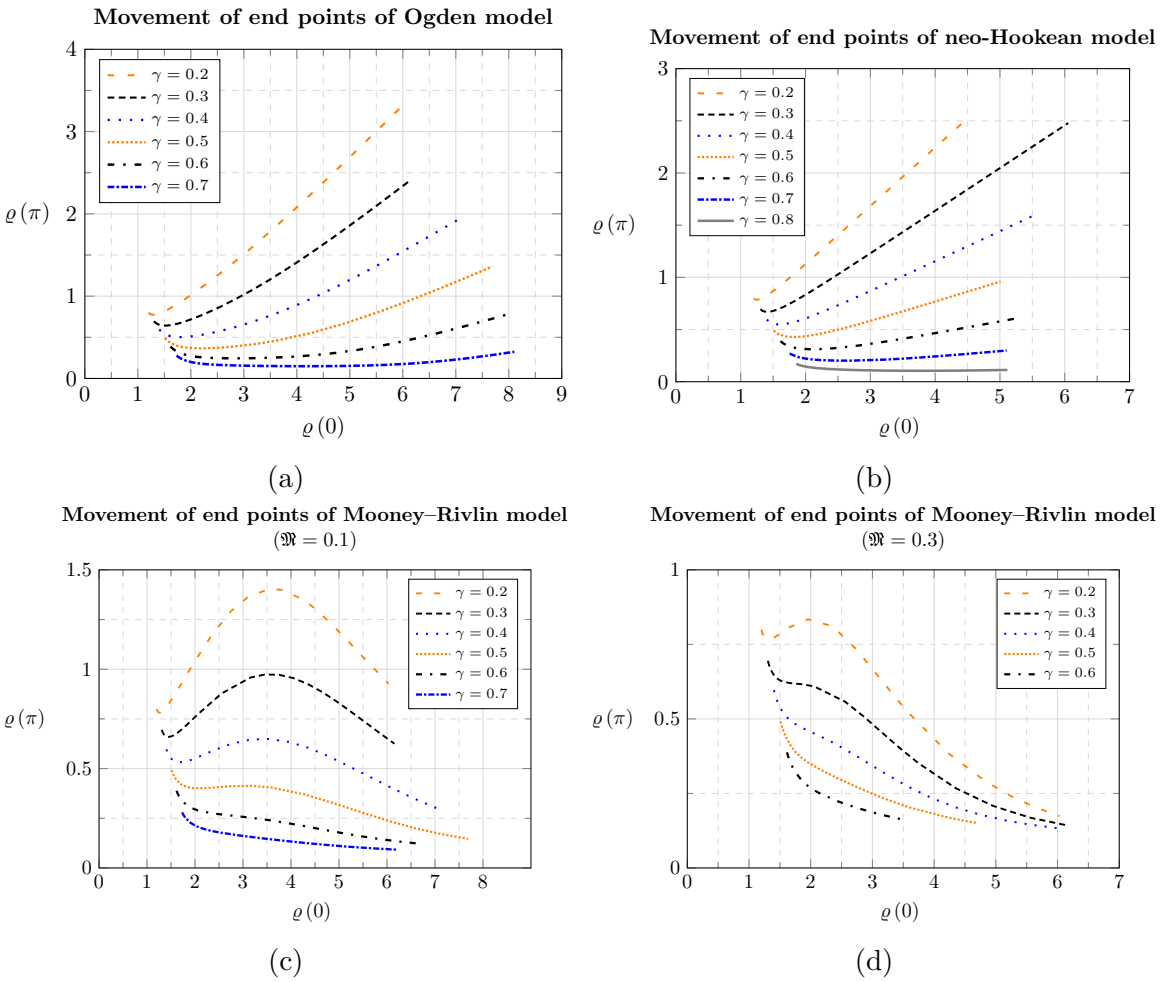

Figure 3: Movement of end points for different hyperelastic constitutive models during inflation of the membrane for various aspect ratios γ. The end $\varrho(0)$ represents the inflation as explained in Section 5.1 and $\varrho(\pi)$ is the inner end of the torus profile.

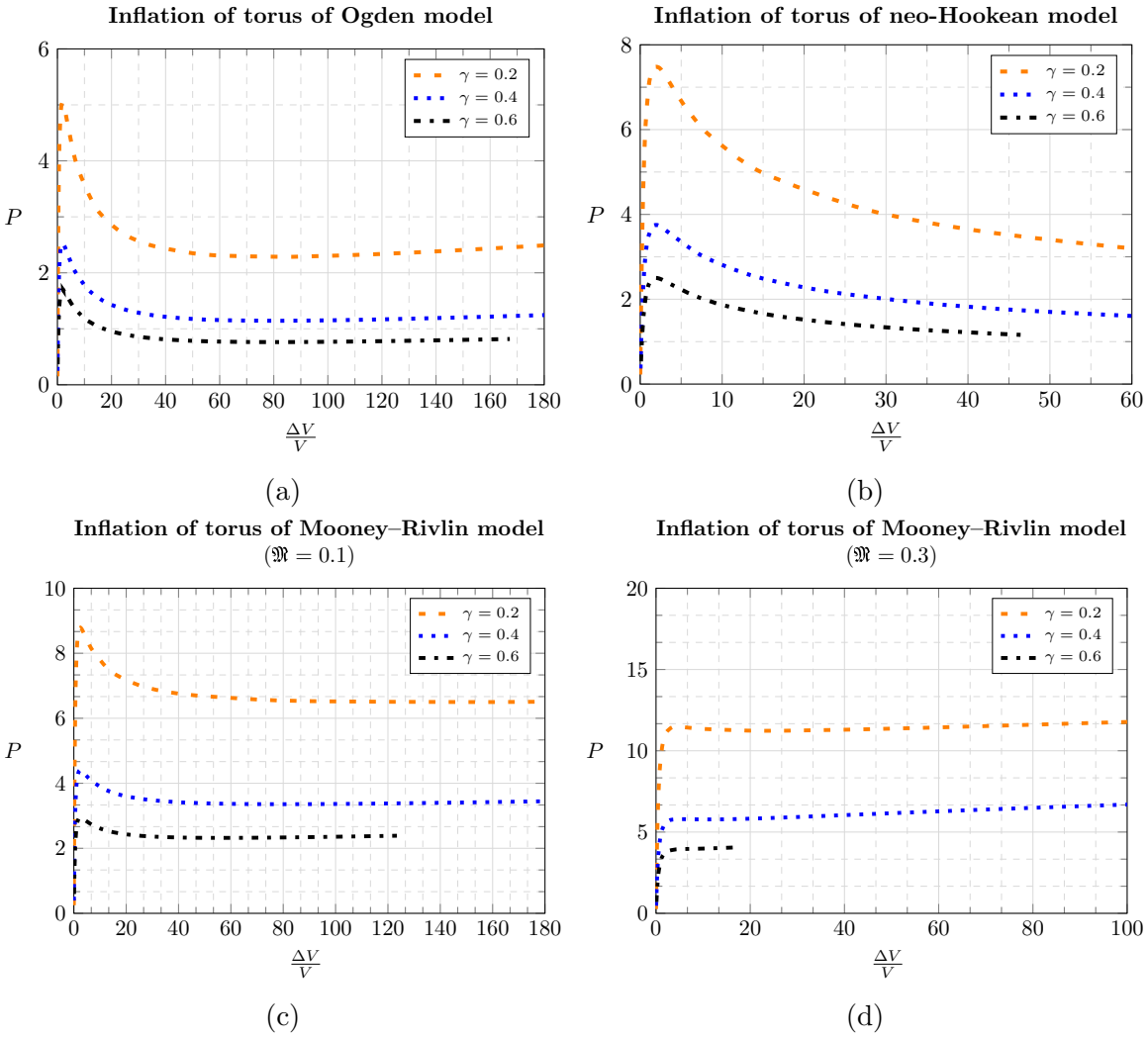

Figure 4: Pressure vs volume curves for all the three material models for three different aspect ratios $\gamma = 0.2, 0.4, 0.6$.

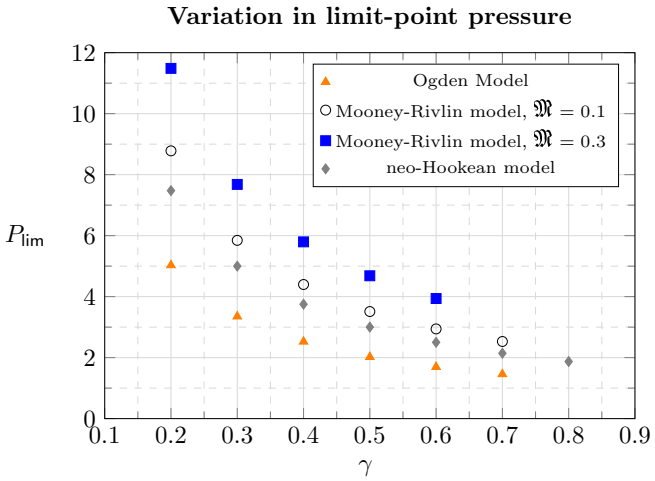

Figure 5: Variation of limit point pressure with aspect ratio for different elastic constitutive models.

higher pressure values for the same relative increase in volume. This effect is also visible in the limit point pressure P_{lim} plotted in Figure 5. Higher values of γ result in lower values of corresponding P_{lim}. We also note that with comparable values of shear modulus μ used in the computations, Ogden material has the smallest value of P_{lim} followed by neo-Hookean and Mooney–Rivlin materials, respectively. We note that upon increasing volume beyond the limit point, there is a consistent decline in pressure for the neo-Hookean model whereas opposite happens for Mooney–Rivlin ($\mathfrak{M} = 0.3, \gamma = 0.6$) case where pressure increases monotonically. In all the other cases (Ogden model, Mooney–Rivlin ($\mathfrak{M} = 0.1$) and Mooney–Rivlin ($\mathfrak{M} = 0.3, \gamma = 0.2, 0.4$)) pressure rises with volume after an initial fall at the limit point.

We also study the variation of Cauchy stresses in the membrane with inflation as computed using equations (43), (47), and (51). The behaviour is almost similar for all the three models and we plot a few representative results for Ogden model in Figure 6. Variation of the principal stresses $\sigma_{\theta\theta}$ and $\sigma_{\phi\phi}$ at the inner equator ($\theta = \pi$) with the internal pressure is shown. Typically the magnitude of principal stresses along the minor circumference ($\sigma_{\theta\theta}$) is larger than that of the principal stresses along the major circumference ($\sigma_{\phi\phi}$). For most cases, the stresses increase monotonically with inflation, the exception being $\sigma_{\phi\phi}(\theta = \pi)$ at $\gamma = \{0.6, 0.7\}$. Beyond the limit point, the stresses increase rapidly upon slight changes in pressure, likely leading to failure.

We further observe in Figure 6 that $\sigma_{\phi\phi}$ attains a negative value for certain values of pressure for torus with $\gamma = 0.7$. Similar observations are made for the neo-Hookean model ($\gamma = 0.8$) and Mooney–Rivlin model ($\{\mathfrak{M} = 0.1; \gamma = 0.4, 0.5, 0.6, 0.7\}$ and $\{\mathfrak{M} = 0.3; \gamma = 0.2, 0.3, 0.4, 0.5, 0.6\}$) but those results are not plotted here for the sake of brevity. Negative values of the principal stress indicate the occurrence of wrinkling instability and this is further explored in Section 5.3.

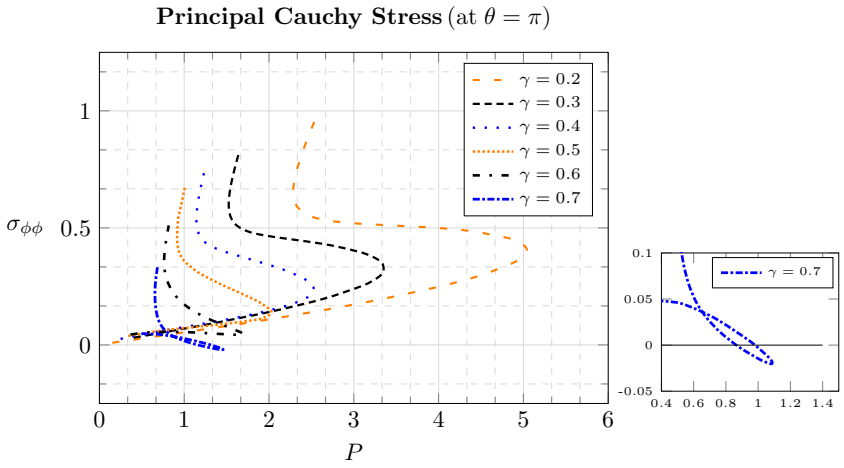

(a)

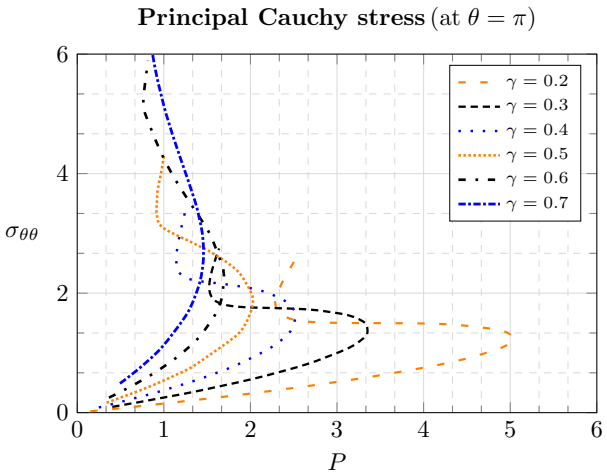

(b)

Figure 6: Variation of the principal stresses $\sigma_{\theta\theta}$ and $\sigma_{\phi\phi}$ with pressure at the inner equator ($\theta = \pi$) of the torus for the Ogden material model.

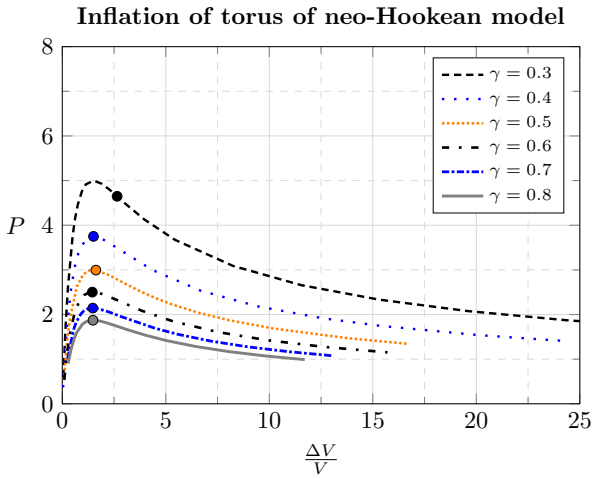

Figure 7: First critical points on the pressure-volume curves for the neo-Hookean model are marked with dots. For $\gamma = 0.3$, critical point is achieved for $n = 2$ and occurs significantly after the limit point, while for all other cases it is achieved at $n = 1$ very close to the limit point.

5.2 Calculation of critical pressure

The fundamental solution obtained for the variables ϱ_θ and η_θ is used in calculating second order derivatives of ϱ and η with respect to the variable θ. The values of $\varrho_{\theta\theta}$ and $\eta_{\theta\theta}$ in each interval are calculated by using forward difference method, i.e. $\varrho_{\theta\theta_i} = (\varrho_{\theta_{i+1}} - \varrho_{\theta_i})/\Delta\theta$ where $\Delta\theta = \pi/2000$ and $i = 1, 2, \ldots 2000$. The variables (ϱ, η) and their derivatives are calculated at each θ_i for all the values of pressure during inflation process of a membrane with an aspect ratio, γ. These values are substituted in equation (35) and by changing the values of the mode number n from 1 to 5, we calculate $\mathcal{R}_{\text{res}}$ at each θ_i for all the values of pressure and for a given aspect ratio γ. We repeat this process for all the values of $\gamma \in (0.2, 0.8)$ considered in our study for the neo-Hookean material. Zeros of $\mathcal{R}_{\text{res}}$ are searched by computing the value of pressure at which it changes sign. Only a change of order $(> \mathcal{O}(10^{-4}))$ in the residual value is considered to be admissible to avoid numerical errors; if the value of $\mathcal{R}_{\text{res}}$ does not fall in the desired range we do not assign any critical value of pressure for that case. This procedure is repeated for the entire domain $\theta \in [0, \pi]$ and the corresponding critical pressure for the point located at θ_i on the membrane is noted. The lowest of all the critical pressure values occurring at or before the limit point for a given aspect ratio is termed as critical point pressure for that membrane under inflation.

Based on our computations, we obtain critical (bifurcation) points for the cases $\{n = 1, \gamma = 0.4, 0.5, 0.6, 0.7, 0.8\}$. and $\{n = 2, \gamma = 0.3\}$. All other cases lead to no solution of equation (35). The critical point for $\gamma = 0.3$ occurs well after the limit point and although this configuration is difficult to access in a pressure controlled experiment, it can be achieved in a volume or mass controlled experiment (Wang et al., 2017). For all other γ values, the critical points are very close (albeit not equal) to the limit point. These points are depicted graphically in Figure 7.

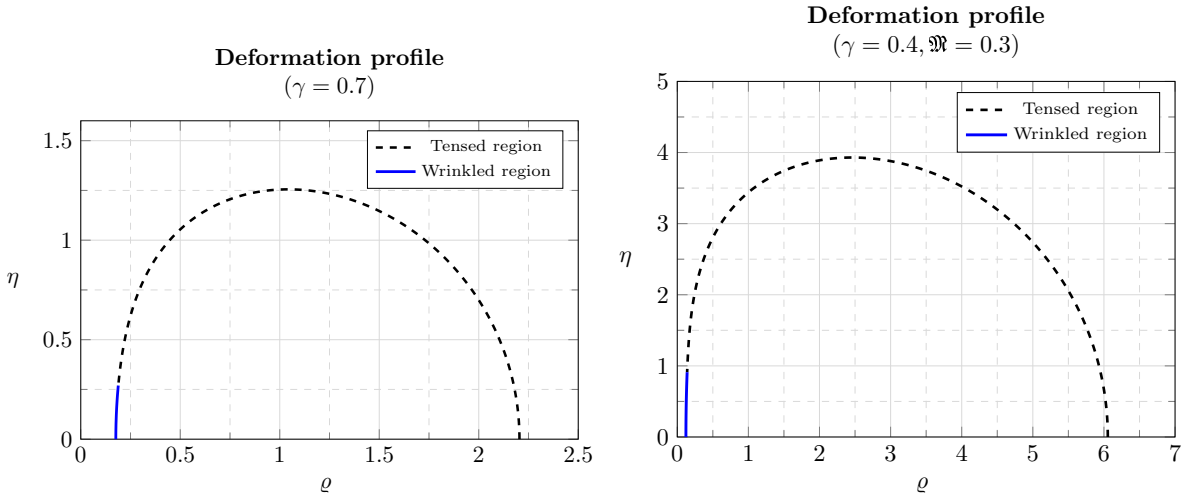

(a) Inflating Pressure: 1.46, $\varrho(0) = 2.20$. (b) Inflating Pressure: 7.62, $\varrho(0) = 6.05$.

Figure 8: Membrane profiles upon wrinkling computed using relaxed strain energy density for (a) Ogden constitutive model and (b) Mooney-Rivlin model, for different inflating pressures.

5.3 Computation of wrinkling instability

Wrinkling is achieved when the in-plane stress in any direction in the membrane reaches zero. In the negative-stress regions, we use the relaxed form of the strain energy density and the subsequently modified equations in Section 3.2 to recompute the solutions with a method similar to that employed in Section 5.1.

We start with an initial guess value for the location of onset of wrinkling region θ_{wr} taken to be the starting location of the region $\sigma_{\phi\phi} < 0$. We employ standard strain energy density in the region $0 \leq \theta \leq \theta_{\text{wr}}$ to calculate the variables $\varrho, \varrho_\theta, \eta$, and η_θ at θ_{wr} and use these as the initial conditions to determine the solution in the region $\theta_{\text{wr}} \leq \theta \leq \pi$ employing the relaxed strain energy density function. Next, we minimize the cost function $\left[\varrho_\theta(\pi)^2 + \eta(\pi)^2\right]^{\frac{1}{2}}$ to a sufficiently small quantity ($< \mathcal{O}(10^{-12})$) by using the Nelder-Mead simplex optimisation technique of two variables $(\eta_\theta(0), P)$ and determine the variables over the domain $\theta \in [0, \pi]$. Then, we calculate $\lambda_2^2\lambda_1 - 1$ obtained at θ_{wr} to check if the value is in order of ($< \mathcal{O}(10^{-10})$) and this process is repeated by varying θ_{wr} in the range $\left(\frac{\pi}{2}, \pi\right)$ till we get the desired solution set (λ_1, λ_2) at θ_{wr}, since we observe that both the principal stretch ratio values are greater than one for the points on the boundary in the range $0 \leq \theta \leq \frac{\pi}{2}$. The coordinate $\theta = \theta_{\text{wr}}$ at which $\lambda_2^2\lambda_1 - 1 < \mathcal{O}(10^{-10})$ represents the starting location of wrinkles on the membrane. This numerical scheme is implemented in Matlab R2017b. We note that this scheme is an improvement over the traditional case where θ_{wr} would simply be taken as the first point where $\sigma_{\phi\phi} < 0$ based on computations made using the standard energy density function.

Wrinkling analysis is carried out for Ogden material with aspect ratio $\gamma = 0.7$, for Mooney–Rivlin material with $\gamma = 0.4, \mathfrak{M} = 0.3$, and for neo-Hookean material with as-

Table 2: Error in the prediction of parameters by standard strain energy density function

Model	Variable	$\varrho\,(0)$	P	Standard energy density	Relaxed energy density	Error %
Ogden ($\gamma = 0.7$)	θ_{wr}	2.01	1.41	173.97°	172.98°	0.57
		2.20	1.46	173.07°	171.81°	0.73
Mooney-Rivlin ($\gamma = 0.4, \mathfrak{M} = 0.3$)	θ_{wr}	5.55	7.23	176.13°	175.41°	0.41
		6.05	7.62	174.42°	173.07°	0.77
neo-Hookean ($\gamma = 0.8$)	θ_{wr}	2.21	1.84	175.41°	174.60°	0.46
		2.31	1.87	175.41°	174.60°	0.46

pect ratio $\gamma = 0.8$ after observing negative $\sigma_{\phi\phi}$ stress values as discussed in Section 5.1.2. We observe that wrinkling occurs only in a small region near the inner equator on the membrane for all the above-mentioned cases whenever $\sigma_{\phi\phi} < 0$. Thus, according to the tension field theory, wrinkling happens along the ϕ direction while the wrinkle lines ought to appear along the θ direction. Membrane profiles upon wrinkling for two cases of Ogden and Mooney–Rivlin models are plotted in Figure 8.

Once the onset of wrinkling is confirmed by observing negative circumferential stress values, we recompute the entire solution using the combination of relaxed and total strain energy densities using the numerical scheme described earlier in this section. We observe that this updated solution (membrane profile and location of wrinkling) is different from the one in which θ_{wr} is obtained using the standard strain energy. Values obtained by both the solutions and relative errors are presented in Table 2. Here $\theta = \theta_{\text{wr}}$ is the starting point of wrinkles in the reference configuration. Maximum error in the calculations of θ_{wr} is 0.77% or 1.3°, for the Mooney–Rivlin material at the pressure $P = 7.62$. Although the error between these two approaches in this case of toroidal geometry is small, the difference in solutions is still noteworthy and might be more relevant in other constitutive models or membrane geometry.

6 Conclusions

In this work we have presented new analysis and results in the study of free inflation of a nonlinear hyperelastic toroidal membrane. To analyse the deformation behaviour and instabilities in free inflation of a torus under a hydrostatic pressure, toroidal membranes made of three materials (Ogden, Mooney–Rivlin, and neo-Hookean) are considered and a comparative study is conducted amongst them. We observe strain-hardening behaviour in Ogden and Mooney–Rivlin material models after the limit point pressure. For the neo-Hookean model bifurcation of solution occurs well post limit point for $\gamma = 0.3$ corresponding to the second mode, and very close to the limit point for all other aspect ratios for the first mode.

We notice that limit point pressure decreases with increase in aspect ratio and increases with increase in stiffness of the membrane. We also notice that for Mooney–Rivlin

model with higher aspect ratio and a stiffer material, non-dimensional pressure increases monotonically with inflation. In the compressive stress regions, we use the concept of relaxed strain energy density to study wrinkling behaviour and we observe differences between the wrinkled configuration predicted by standard strain energy density and its relaxed form.

Based on our results on critical point bifurcation and wrinkling, it can be claimed that the predicted behaviour of membrane in Figure 4 and Figure 6 for large volume cases is most likely inaccurate. The fundamental solution does not hold for the post-instability regime and a recalculation of configuration/ stress/ pressure needs to be performed. This post-buckling analysis to understand membrane's behaviour will be undertaken as future work.

Acknowledgements
Major portion of this work was conducted when both the authors were based at IIT Hyderabad. This work was financially supported by a research grant associated with the Ramanujan fellowship by the Science and Engineering Research Board (Sanction No: SB/S2/RJN-116/2015) awarded to PS.

A Matrix coefficients of governing equations for various constitutive models

A.1 Coefficients for Ogden model

For Ogden constitutive model, the governing equation (8) gives

$$\sum_{j=1}^{3} \frac{\mu_j}{\lambda_1^{\alpha_j+3}\lambda_2^{\alpha_j+1}\gamma^{2\alpha_j+2}R^{2\alpha_j+2}\left[\varrho_\theta^2+\eta_\theta^2\right]^{\frac{3}{2}}}\left[\widehat{A}_j\varrho_{\theta\theta}+\widehat{B}_j\eta_{\theta\theta}+\widehat{C}_j\right]+\left[\frac{\widetilde{P}R_b}{T}\right]\varrho\eta_\theta=0, \quad (36)$$

while the governing equation (9) results in

$$\sum_{j=1}^{3} \frac{\mu_j}{\lambda_1^{\alpha_j+3}\lambda_2^{\alpha_j+1}\gamma^{2\alpha_j+2}R^{2\alpha_j+2}\left[\varrho_\theta^2+\eta_\theta^2\right]^{\frac{3}{2}}}\left[\widehat{D}_j\varrho_{\theta\theta}+\widehat{E}_j\eta_{\theta\theta}+\widehat{F}_j\right]-\left[\frac{\widetilde{P}R_b}{T}\right]\varrho\varrho_\theta=0, \quad (37)$$

where,

$$
\begin{aligned}
\widehat{A}_j &= \Big[\big[\alpha_j-1\big]\big[\varrho_\theta^2+\eta_\theta^2\big]^{\alpha_j}\varrho^{\alpha_j}R^{\alpha_j}+\big[\alpha_j+1\big]\gamma^{2\alpha_j}R^{2\alpha_j}\Big]\varrho_\theta^2\Big[\varrho_\theta^2+\eta_\theta^2\Big]\varrho R^2\\
&+\Big[\big[\varrho_\theta^2+\eta_\theta^2\big]^{\alpha_j}\varrho^{\alpha_j}R^{\alpha_j}-\gamma^{2\alpha_j}R^{2\alpha_j}\Big]\eta_\theta^2\Big[\varrho_\theta^2+\eta_\theta^2\Big]\varrho R^2,\\
\widehat{B}_j &= \Big[\big[\alpha_j-1\big]\big[\varrho_\theta^2+\eta_\theta^2\big]^{\alpha_j}\varrho^{\alpha_j}R^{\alpha_j}+\big[\alpha_j+1\big]\gamma^{2\alpha_j}R^{2\alpha_j}\Big]\varrho_\theta\eta_\theta\Big[\varrho_\theta^2+\eta_\theta^2\Big]\varrho R^2\\
&-\Big[\big[\varrho_\theta^2+\eta_\theta^2\big]^{\alpha_j}\varrho^{\alpha_j}R^{\alpha_j}-\gamma^{2\alpha_j}R^{2\alpha_j}\Big]\varrho_\theta\eta_\theta\Big[\varrho_\theta^2+\eta_\theta^2\Big]\varrho R^2,\\
\widehat{C}_j &= \alpha_j\Big[\varrho_\theta R+\varrho\gamma\sin\theta\Big]\varrho_\theta\Big[\varrho_\theta^2+\eta_\theta^2\Big]^2\gamma^{2\alpha_j}R^{2\alpha_j+1}\\
&-\Big[\big[\varrho_\theta^2+\eta_\theta^2\big]^{\alpha_j}\varrho^{\alpha_j}R^{\alpha_j}-\gamma^{2\alpha_j}R^{2\alpha_j}\Big]\varrho\varrho_\theta\Big[\varrho_\theta^2+\eta_\theta^2\Big]^2\gamma R\sin\theta\\
&-\Big[\big[\varrho_\theta^2+\eta_\theta^2\big]^{\frac{\alpha_j}{2}}\varrho^{2\alpha_j}\gamma^{\alpha_j}-\gamma^{2\alpha_j}R^{2\alpha_j}\Big]\Big[\varrho_\theta^2+\eta_\theta^2\Big]^3R^2,
\end{aligned}
\tag{38}
$$

and

$$
\begin{aligned}
\widehat{D}_j &= \Big[\big[\alpha_j-1\big]\big[\varrho_\theta^2+\eta_\theta^2\big]^{\alpha_j}\varrho^{\alpha_j}R^{\alpha_j}+\big[\alpha_j+1\big]\gamma^{2\alpha_j}R^{2\alpha_j}\Big]\varrho_\theta\eta_\theta\Big[\varrho_\theta^2+\eta_\theta^2\Big]\varrho R^2\\
&-\Big[\big[\varrho_\theta^2+\eta_\theta^2\big]^{\alpha_j}\varrho^{\alpha_j}R^{\alpha_j}-\gamma^{2\alpha_j}R^{2\alpha_j}\Big]\varrho_\theta\eta_\theta\Big[\varrho_\theta^2+\eta_\theta^2\Big]\varrho R^2,\\
\widehat{E}_j &= \Big[\big[\alpha_j-1\big]\big[\varrho_\theta^2+\eta_\theta^2\big]^{\alpha_j}\varrho^{\alpha_j}R^{\alpha_j}+\big[\alpha_j+1\big]\gamma^{2\alpha_j}R^{2\alpha_j}\Big]\eta_\theta^2\Big[\varrho_\theta^2+\eta_\theta^2\Big]\varrho R^2\\
&+\Big[\big[\varrho_\theta^2+\eta_\theta^2\big]^{\alpha_j}\varrho^{\alpha_j}R^{\alpha_j}-\gamma^{2\alpha_j}R^{2\alpha_j}\Big]\varrho_\theta^2\Big[\varrho_\theta^2+\eta_\theta^2\Big]\varrho R^2,\\
\widehat{F}_j &= \alpha_j\Big[\varrho_\theta R+\varrho\gamma\sin\theta\Big]\eta_\theta\Big[\varrho_\theta^2+\eta_\theta^2\Big]^2\gamma^{2\alpha_j}R^{2\alpha_j+1}\\
&-\Big[\big[\varrho_\theta^2+\eta_\theta^2\big]^{\alpha_j}\varrho^{\alpha_j}R^{\alpha_j}-\gamma^{2\alpha_j}R^{2\alpha_j}\Big]\varrho\eta_\theta\Big[\varrho_\theta^2+\eta_\theta^2\Big]^2\gamma R\sin\theta.
\end{aligned}
\tag{39}
$$

The components of matrices in equation (14) for the Ogden energy density are given by

$$
\begin{aligned}
\mathcal{S}_{22} &= \mu_1^* \left[\mathcal{U}_1 R^2 \left[\mathcal{U}_2^2 + \mathcal{U}_4^2 \right] \left[\left[\mathcal{S}^1 \right] \mathcal{U}_2^2 + \left[\mathcal{S}^2 \right] \mathcal{U}_4^2 \right] \right] \lambda_1^{\alpha_2+\alpha_3+6} \lambda_2^{\alpha_2+\alpha_3+2} \gamma^{2\alpha_2+2\alpha_3+4} R^{2\alpha_2+2\alpha_3+4} \\
&+ \mu_2^* \left[\mathcal{U}_1 R^2 \left[\mathcal{U}_2^2 + \mathcal{U}_4^2 \right] \left[\left[\mathcal{S}^3 \right] \mathcal{U}_2^2 + \left[\mathcal{S}^4 \right] \mathcal{U}_4^2 \right] \right] \lambda_1^{\alpha_1+\alpha_3+6} \lambda_2^{\alpha_1+\alpha_3+2} \gamma^{2\alpha_1+2\alpha_3+4} R^{2\alpha_1+2\alpha_3+4} \\
&+ \mu_3^* \left[\mathcal{U}_1 R^2 \left[\mathcal{U}_2^2 + \mathcal{U}_4^2 \right] \left[\left[\mathcal{S}^5 \right] \mathcal{U}_2^2 + \left[\mathcal{S}^6 \right] \mathcal{U}_4^2 \right] \right] \lambda_1^{\alpha_1+\alpha_2+6} \lambda_2^{\alpha_1+\alpha_2+2} \gamma^{2\alpha_1+2\alpha_2+4} R^{2\alpha_1+2\alpha_2+4}, \\
\mathcal{S}_{24} &= \mu_1^* \left[\mathcal{U}_1 R^2 \left[\mathcal{U}_2^2 + \mathcal{U}_4^2 \right] \left[\left[\mathcal{S}^1 \right] \mathcal{U}_2 \mathcal{U}_4 - \left[\mathcal{S}^2 \right] \mathcal{U}_2 \mathcal{U}_4 \right] \right] \lambda_1^{\alpha_2+\alpha_3+6} \lambda_2^{\alpha_2+\alpha_3+2} \gamma^{2\alpha_2+2\alpha_3+4} R^{2\alpha_2+2\alpha_3+4} \\
&+ \mu_2^* \left[\mathcal{U}_1 R^2 \left[\mathcal{U}_2^2 + \mathcal{U}_4^2 \right] \left[\left[\mathcal{S}^3 \right] \mathcal{U}_2 \mathcal{U}_4 - \left[\mathcal{S}^4 \right] \mathcal{U}_2 \mathcal{U}_4 \right] \right] \lambda_1^{\alpha_1+\alpha_3+6} \lambda_2^{\alpha_1+\alpha_3+2} \gamma^{2\alpha_1+2\alpha_3+4} R^{2\alpha_1+2\alpha_3+4} \\
&+ \mu_3^* \left[\mathcal{U}_1 R^2 \left[\mathcal{U}_2^2 + \mathcal{U}_4^2 \right] \left[\left[\mathcal{S}^5 \right] \mathcal{U}_2 \mathcal{U}_4 - \left[\mathcal{S}^6 \right] \mathcal{U}_2 \mathcal{U}_4 \right] \right] \lambda_1^{\alpha_1+\alpha_2+6} \lambda_2^{\alpha_1+\alpha_2+2} \gamma^{2\alpha_1+2\alpha_2+4} R^{2\alpha_1+2\alpha_2+4}, \\
\mathcal{S}_{42} &= \mu_1^* \left[\mathcal{U}_1 R^2 \left[\mathcal{U}_2^2 + \mathcal{U}_4^2 \right] \left[\left[\mathcal{S}^1 \right] \mathcal{U}_2 \mathcal{U}_4 - \left[\mathcal{S}^2 \right] \mathcal{U}_2 \mathcal{U}_4 \right] \right] \lambda_1^{\alpha_2+\alpha_3+6} \lambda_2^{\alpha_2+\alpha_3+2} \gamma^{2\alpha_2+2\alpha_3+4} R^{2\alpha_2+2\alpha_3+4} \\
&+ \mu_2^* \left[\mathcal{U}_1 R^2 \left[\mathcal{U}_2^2 + \mathcal{U}_4^2 \right] \left[\left[\mathcal{S}^3 \right] \mathcal{U}_2 \mathcal{U}_4 - \left[\mathcal{S}^4 \right] \mathcal{U}_2 \mathcal{U}_4 \right] \right] \lambda_1^{\alpha_1+\alpha_3+6} \lambda_2^{\alpha_1+\alpha_3+2} \gamma^{2\alpha_1+2\alpha_3+4} R^{2\alpha_1+2\alpha_3+4} \\
&+ \mu_3^* \left[\mathcal{U}_1 R^2 \left[\mathcal{U}_2^2 + \mathcal{U}_4^2 \right] \left[\left[\mathcal{S}^5 \right] \mathcal{U}_2 \mathcal{U}_4 - \left[\mathcal{S}^6 \right] \mathcal{U}_2 \mathcal{U}_4 \right] \right] \lambda_1^{\alpha_1+\alpha_2+6} \lambda_2^{\alpha_1+\alpha_2+2} \gamma^{2\alpha_1+2\alpha_2+4} R^{2\alpha_1+2\alpha_2+4}, \\
\mathcal{S}_{44} &= \mu_1^* \left[\mathcal{U}_1 R^2 \left[\mathcal{U}_2^2 + \mathcal{U}_4^2 \right] \left[\left[\mathcal{S}^1 \right] \mathcal{U}_4^2 + \left[\mathcal{S}^2 \right] \mathcal{U}_2^2 \right] \right] \lambda_1^{\alpha_2+\alpha_3+6} \lambda_2^{\alpha_2+\alpha_3+2} \gamma^{2\alpha_2+2\alpha_3+4} R^{2\alpha_2+2\alpha_3+4} \\
&+ \mu_2^* \left[\mathcal{U}_1 R^2 \left[\mathcal{U}_2^2 + \mathcal{U}_4^2 \right] \left[\left[\mathcal{S}^3 \right] \mathcal{U}_4^2 + \left[\mathcal{S}^4 \right] \mathcal{U}_2^2 \right] \right] \lambda_1^{\alpha_1+\alpha_3+6} \lambda_2^{\alpha_1+\alpha_3+2} \gamma^{2\alpha_1+2\alpha_3+4} R^{2\alpha_1+2\alpha_3+4} \\
&+ \mu_3^* \left[\mathcal{U}_1 R^2 \left[\mathcal{U}_2^2 + \mathcal{U}_4^2 \right] \left[\left[\mathcal{S}^5 \right] \mathcal{U}_4^2 + \left[\mathcal{S}^6 \right] \mathcal{U}_2^2 \right] \right] \lambda_1^{\alpha_1+\alpha_2+6} \lambda_2^{\alpha_1+\alpha_2+2} \gamma^{2\alpha_1+2\alpha_2+4} R^{2\alpha_1+2\alpha_2+4},
\end{aligned}
\tag{40}
$$

and

$$
\begin{aligned}
\mathcal{V}_1 &= \mu_1^*\left[\left[\mathcal{V}^2\right]\mathcal{U}_1\mathcal{U}_2\left[\mathcal{U}_2^2+\mathcal{U}_4^2\right]^2\gamma R\sin\theta+\left[\mathcal{V}^7\right]\left[\mathcal{U}_2^2+\mathcal{U}_4^2\right]^3R^2\right]\lambda_1^{\alpha_2+\alpha_3+6}\lambda_2^{\alpha_2+\alpha_3+2}\gamma^{2\alpha_2+2\alpha_3+4}R^{2\alpha_2+2\alpha_3+4}\\
&\quad-\mu_1^*\left[\left[\mathcal{V}^1\right]\mathcal{U}_2\left[\mathcal{U}_2^2+\mathcal{U}_4^2\right]^2\right]\lambda_1^{\alpha_2+\alpha_3+6}\lambda_2^{\alpha_2+\alpha_3+2}\gamma^{2\alpha_2+2\alpha_3+4}R^{2\alpha_2+2\alpha_3+4}\\
&\quad+\mu_2^*\left[\left[\mathcal{V}^4\right]\mathcal{U}_1\mathcal{U}_2\left[\mathcal{U}_2^2+\mathcal{U}_4^2\right]^2\gamma R\sin\theta+\left[\mathcal{V}^8\right]\left[\mathcal{U}_2^2+\mathcal{U}_4^2\right]^3R^2\right]\lambda_1^{\alpha_1+\alpha_3+6}\lambda_2^{\alpha_1+\alpha_3+2}\gamma^{2\alpha_1+2\alpha_3+4}R^{2\alpha_1+2\alpha_3+4}\\
&\quad-\mu_2^*\left[\left[\mathcal{V}^3\right]\mathcal{U}_2\left[\mathcal{U}_2^2+\mathcal{U}_4^2\right]^2\right]\lambda_1^{\alpha_1+\alpha_3+6}\lambda_2^{\alpha_1+\alpha_3+2}\gamma^{2\alpha_1+2\alpha_3+4}R^{2\alpha_1+2\alpha_3+4}\\
&\quad+\mu_3^*\left[\left[\mathcal{V}^6\right]\mathcal{U}_1\mathcal{U}_2\left[\mathcal{U}_2^2+\mathcal{U}_4^2\right]^2\gamma R\sin\theta+\left[\mathcal{V}^9\right]\left[\mathcal{U}_2^2+\mathcal{U}_4^2\right]^3R^2\right]\lambda_1^{\alpha_1+\alpha_2+6}\lambda_2^{\alpha_1+\alpha_2+2}\gamma^{2\alpha_1+2\alpha_2+4}R^{2\alpha_1+2\alpha_2+4}\\
&\quad-\mu_3^*\left[\left[\mathcal{V}^5\right]\mathcal{U}_2\left[\mathcal{U}_2^2+\mathcal{U}_4^2\right]^2\right]\lambda_1^{\alpha_1+\alpha_2+6}\lambda_2^{\alpha_1+\alpha_2+2}\gamma^{2\alpha_1+2\alpha_2+4}R^{2\alpha_1+2\alpha_2+4}\\
&\quad-\frac{\mu_1^*}{2}P\mathcal{U}_1\mathcal{U}_4\left[\mathcal{U}_2^2+\mathcal{U}_4^2\right]^{\frac{3}{2}}\lambda_1^{\alpha_1+\alpha_2+\alpha_3+9}\lambda_2^{\alpha_1+\alpha_2+\alpha_3+3}\gamma^{2\alpha_1+2\alpha_2+2\alpha_3+6}R^{2\alpha_1+2\alpha_2+2\alpha_3+6},\\
\mathcal{V}_2 &= \mu_1^*\left[\left[\mathcal{V}^2\right]\mathcal{U}_1\mathcal{U}_4\left[\mathcal{U}_2^2+\mathcal{U}_4^2\right]^2\gamma R\sin\theta\right]\lambda_1^{\alpha_2+\alpha_3+6}\lambda_2^{\alpha_2+\alpha_3+2}\gamma^{2\alpha_2+2\alpha_3+4}R^{2\alpha_2+2\alpha_3+4}\\
&\quad-\mu_1^*\left[\left[\mathcal{V}^1\right]\mathcal{U}_4\left[\mathcal{U}_2^2+\mathcal{U}_4^2\right]^2\right]\lambda_1^{\alpha_2+\alpha_3+6}\lambda_2^{\alpha_2+\alpha_3+2}\gamma^{2\alpha_2+2\alpha_3+4}R^{2\alpha_2+2\alpha_3+4}\\
&\quad+\mu_2^*\left[\left[\mathcal{V}^4\right]\mathcal{U}_1\mathcal{U}_4\left[\mathcal{U}_2^2+\mathcal{U}_4^2\right]^2\gamma R\sin\theta\right]\lambda_1^{\alpha_1+\alpha_3+6}\lambda_2^{\alpha_1+\alpha_3+2}\gamma^{2\alpha_1+2\alpha_3+4}R^{2\alpha_1+2\alpha_3+4}\\
&\quad-\mu_2^*\left[\left[\mathcal{V}^3\right]\mathcal{U}_4\left[\mathcal{U}_2^2+\mathcal{U}_4^2\right]^2\right]\lambda_1^{\alpha_1+\alpha_3+6}\lambda_2^{\alpha_1+\alpha_3+2}\gamma^{2\alpha_1+2\alpha_3+4}R^{2\alpha_1+2\alpha_3+4}\\
&\quad+\mu_3^*\left[\left[\mathcal{V}^6\right]\mathcal{U}_1\mathcal{U}_4\left[\mathcal{U}_2^2+\mathcal{U}_4^2\right]^2\gamma R\sin\theta\right]\lambda_1^{\alpha_1+\alpha_2+6}\lambda_2^{\alpha_1+\alpha_2+2}\gamma^{2\alpha_1+2\alpha_2+4}R^{2\alpha_1+2\alpha_2+4}\\
&\quad-\mu_3^*\left[\left[\mathcal{V}^5\right]\mathcal{U}_4\left[\mathcal{U}_2^2+\mathcal{U}_4^2\right]^2\right]\lambda_1^{\alpha_1+\alpha_2+6}\lambda_2^{\alpha_1+\alpha_2+2}\gamma^{2\alpha_1+2\alpha_2+4}R^{2\alpha_1+2\alpha_2+4}\\
&\quad+\frac{\mu_1^*}{2}P\mathcal{U}_1\mathcal{U}_2\left[\mathcal{U}_2^2+\mathcal{U}_4^2\right]^{\frac{3}{2}}\lambda_1^{\alpha_1+\alpha_2+\alpha_3+9}\lambda_2^{\alpha_1+\alpha_2+\alpha_3+3}\gamma^{2\alpha_1+2\alpha_2+2\alpha_3+6}R^{2\alpha_1+2\alpha_2+2\alpha_3+6},
\end{aligned}
\tag{41}
$$

along with

$$
\begin{aligned}
\mathcal{S}^1 &= \big[\alpha_1 - 1\big]\big[\mathcal{U}_2^2 + \mathcal{U}_4^2\big]^{\alpha_1}\mathcal{U}_1^{\alpha_1} R^{\alpha_1} + \big[\alpha_1 + 1\big]\gamma^{2\alpha_1} R^{2\alpha_1}, & \mathcal{S}^2 &= \big[\mathcal{U}_2^2 + \mathcal{U}_4^2\big]^{\alpha_1}\mathcal{U}_1^{\alpha_1} R^{\alpha_1} - \gamma^{2\alpha_1} R^{2\alpha_1},\\
\mathcal{S}^3 &= \big[\alpha_2 - 1\big]\big[\mathcal{U}_2^2 + \mathcal{U}_4^2\big]^{\alpha_2}\mathcal{U}_1^{\alpha_2} R^{\alpha_2} + \big[\alpha_2 + 1\big]\gamma^{2\alpha_2} R^{2\alpha_2}, & \mathcal{S}^4 &= \big[\mathcal{U}_2^2 + \mathcal{U}_4^2\big]^{\alpha_2}\mathcal{U}_1^{\alpha_2} R^{\alpha_2} - \gamma^{2\alpha_2} R^{2\alpha_2},\\
\mathcal{S}^5 &= \big[\alpha_3 - 1\big]\big[\mathcal{U}_2^2 + \mathcal{U}_4^2\big]^{\alpha_3}\mathcal{U}_1^{\alpha_3} R^{\alpha_3} + \big[\alpha_3 + 1\big]\gamma^{2\alpha_3} R^{2\alpha_3}, & \mathcal{S}^6 &= \big[\mathcal{U}_2^2 + \mathcal{U}_4^2\big]^{\alpha_3}\mathcal{U}_1^{\alpha_3} R^{\alpha_3} - \gamma^{2\alpha_3} R^{2\alpha_3},\\
\mathcal{V}^1 &= \alpha_1\big[\mathcal{U}_2 R + \mathcal{U}_1\gamma\sin\theta\big]\gamma^{2\alpha_1} R^{2\alpha_1+1}, & \mathcal{V}^2 &= \big[\mathcal{U}_2^2 + \mathcal{U}_4^2\big]^{\alpha_1}\mathcal{U}_1^{\alpha_1} R^{\alpha_1} - \gamma^{2\alpha_1} R^{2\alpha_1},\\
\mathcal{V}^3 &= \alpha_2\big[\mathcal{U}_2 R + \mathcal{U}_1\gamma\sin\theta\big]\gamma^{2\alpha_2} R^{2\alpha_2+1}, & \mathcal{V}^4 &= \big[\mathcal{U}_2^2 + \mathcal{U}_4^2\big]^{\alpha_2}\mathcal{U}_1^{\alpha_2} R^{\alpha_2} - \gamma^{2\alpha_2} R^{2\alpha_2},\\
\mathcal{V}^5 &= \alpha_3\big[\mathcal{U}_2 R + \mathcal{U}_1\gamma\sin\theta\big]\gamma^{2\alpha_3} R^{2\alpha_3+1}, & \mathcal{V}^6 &= \big[\mathcal{U}_2^2 + \mathcal{U}_4^2\big]^{\alpha_3}\mathcal{U}_1^{\alpha_3} R^{\alpha_3} - \gamma^{2\alpha_3} R^{2\alpha_3},\\
\mathcal{V}^7 &= \big[\mathcal{U}_2^2 + \mathcal{U}_4^2\big]^{\frac{\alpha_1}{2}}\mathcal{U}_1^{2\alpha_1}\gamma^{\alpha_1} - \gamma^{2\alpha_1} R^{2\alpha_1}, & \mathcal{V}^8 &= \big[\mathcal{U}_2^2 + \mathcal{U}_4^2\big]^{\frac{\alpha_2}{2}}\mathcal{U}_1^{2\alpha_2}\gamma^{\alpha_2} - \gamma^{2\alpha_2} R^{2\alpha_2},\\
\mathcal{V}^9 &= \big[\mathcal{U}_2^2 + \mathcal{U}_4^2\big]^{\frac{\alpha_3}{2}}\mathcal{U}_1^{2\alpha_3}\gamma^{\alpha_3} - \gamma^{2\alpha_3} R^{2\alpha_3},\\
P &= \frac{2\widetilde{P} R_b}{\mu_1 T}.
\end{aligned}
\tag{42}
$$

Non-dimensional principal Cauchy stresses in the θ and ϕ-directions are computed as

$$
\sigma_{\theta\theta} = \left[\frac{\lambda_3\alpha_1}{\mu_1^*}\right]\left[\sum_{j=1}^{3}\mu_j^*\lambda_1^{\alpha_j} - \sum_{j=1}^{3}\mu_j^*\lambda_3^{\alpha_j}\right], \quad \sigma_{\phi\phi} = \left[\frac{\lambda_3\alpha_1}{\mu_1^*}\right]\left[\sum_{j=1}^{3}\mu_j^*\lambda_2^{\alpha_j} - \sum_{j=1}^{3}\mu_j^*\lambda_3^{\alpha_j}\right]. \tag{43}
$$

A.2 Coefficients for Mooney–Rivlin model

The components of matrices in equation (14) for the Mooney–Rivlin energy density are given by

$$
\begin{aligned}
\mathcal{S}_{22} &= \left[\mathcal{U}_1 R^2\left[\mathcal{U}_2^2 + \mathcal{U}_4^2\right]\left[\left[\mathcal{S}_m^1\right]\mathcal{U}_2^2 + \left[\mathcal{S}_m^2\right]\mathcal{U}_4^2\right]\right]\lambda_1^4 - \mathfrak{R}\left[\mathcal{U}_1 R^2\left[\mathcal{U}_2^2 + \mathcal{U}_4^2\right]\left[\left[\mathcal{S}_m^3\right]\mathcal{U}_2^2 + \left[\mathcal{S}_m^4\right]\mathcal{U}_4^2\right]\right]\lambda_1^8\lambda_2^4\gamma^8 R^8,\\
\mathcal{S}_{24} &= \left[\mathcal{U}_1 R^2\left[\mathcal{U}_2^2 + \mathcal{U}_4^2\right]\left[\left[\mathcal{S}_m^1\right]\mathcal{U}_2\mathcal{U}_4 - \left[\mathcal{S}_m^2\right]\mathcal{U}_2\mathcal{U}_4\right]\right]\lambda_1^4\\
&\quad - \mathfrak{R}\left[\mathcal{U}_1 R^2\left[\mathcal{U}_2^2 + \mathcal{U}_4^2\right]\left[\left[\mathcal{S}_m^3\right]\mathcal{U}_2\mathcal{U}_4 - \left[\mathcal{S}_m^4\right]\mathcal{U}_2\mathcal{U}_4\right]\right]\lambda_1^8\lambda_2^4\gamma^8 R^8,\\
\mathcal{S}_{42} &= \mathcal{S}_{24},\\
\mathcal{S}_{44} &= \left[\mathcal{U}_1 R^2\left[\mathcal{U}_2^2 + \mathcal{U}_4^2\right]\left[\left[\mathcal{S}_m^1\right]\mathcal{U}_4^2 + \left[\mathcal{S}_m^2\right]\mathcal{U}_2^2\right]\right]\lambda_1^4 - \mathfrak{R}\left[\mathcal{U}_1 R^2\left[\mathcal{U}_2^2 + \mathcal{U}_4^2\right]\left[\left[\mathcal{S}_m^3\right]\mathcal{U}_4^2 + \left[\mathcal{S}_m^4\right]\mathcal{U}_2^2\right]\right]\lambda_1^8\lambda_2^4\gamma^8 R^8,
\end{aligned}
\tag{44}
$$

and

$$\begin{aligned}
\mathcal{V}_1 &= \left[\left[\mathcal{V}_m^2\right]\mathcal{U}_1\mathcal{U}_2\left[\mathcal{U}_2^2+\mathcal{U}_4^2\right]^2\gamma R\sin\theta+\left[\mathcal{V}_m^5\right]\left[\mathcal{U}_2^2+\mathcal{U}_4^2\right]^3R^2\right]\lambda_1^4-\left[\left[\mathcal{V}_m^1\right]\mathcal{U}_2\left[\mathcal{U}_2^2+\mathcal{U}_4^2\right]^2\right]\lambda_1^4\\
&-\mathfrak{M}\left[\left[\mathcal{V}_m^4\right]\mathcal{U}_1\mathcal{U}_2\left[\mathcal{U}_2^2+\mathcal{U}_4^2\right]^2\gamma R\sin\theta+\left[\mathcal{V}_m^6\right]\left[\mathcal{U}_2^2+\mathcal{U}_4^2\right]^3R^2\right]\lambda_1^8\lambda_2^4\gamma^8R^8\\
&+\mathfrak{M}\left[\left[\mathcal{V}_m^3\right]\mathcal{U}_2\left[\mathcal{U}_2^2+\mathcal{U}_4^2\right]^2\right]\lambda_1^8\lambda_2^4\gamma^8R^8-\frac{P}{2}\mathcal{U}_1\mathcal{U}_4\left[\mathcal{U}_2^2+\mathcal{U}_4^2\right]^{\frac{3}{2}}\lambda_1^9\lambda_2^3\gamma^6R^6,\\
\mathcal{V}_2 &= \left[\left[\mathcal{V}_m^2\right]\mathcal{U}_1\mathcal{U}_4\left[\mathcal{U}_2^2+\mathcal{U}_4^2\right]^2\gamma R\sin\theta\right]\lambda_1^4-\left[\left[\mathcal{V}_m^1\right]\mathcal{U}_4\left[\mathcal{U}_2^2+\mathcal{U}_4^2\right]^2\right]\lambda_1^4\\
&-\mathfrak{M}\left[\left[\mathcal{V}_m^4\right]\mathcal{U}_1\mathcal{U}_4\left[\mathcal{U}_2^2+\mathcal{U}_4^2\right]^2\gamma R\sin\theta\right]\lambda_1^8\lambda_2^4\gamma^8R^8\\
&+\mathfrak{M}\left[\left[\mathcal{V}_m^3\right]\mathcal{U}_4\left[\mathcal{U}_2^2+\mathcal{U}_4^2\right]^2\right]\lambda_1^8\lambda_2^4\gamma^8R^8+\frac{P}{2}\mathcal{U}_1\mathcal{U}_2\left[\mathcal{U}_2^2+\mathcal{U}_4^2\right]^{\frac{3}{2}}\lambda_1^9\lambda_2^3\gamma^6R^6,
\end{aligned}\tag{45}$$

along with

$$\begin{aligned}
&\mathcal{S}_m^1=\left[\mathcal{U}_2^2+\mathcal{U}_4^2\right]^2\mathcal{U}_1^2R^2+3\gamma^4R^4, && \mathcal{S}_m^2=\left[\mathcal{U}_2^2+\mathcal{U}_4^2\right]^2\mathcal{U}_1^2R^2-\gamma^4R^4,\\
&\mathcal{S}_m^3=-3\left[\mathcal{U}_2^2+\mathcal{U}_4^2\right]^{-2}\mathcal{U}_1^{-2}R^{-2}-\gamma^{-4}R^{-4}, && \mathcal{S}_m^4=\left[\mathcal{U}_2^2+\mathcal{U}_4^2\right]^{-2}\mathcal{U}_1^{-2}R^{-2}-\gamma^{-4}R^{-4},\\
&\mathcal{V}_m^1=2\left[\mathcal{U}_2R+\mathcal{U}_1\gamma\sin\theta\right]\gamma^4R^5, && \mathcal{V}_m^2=\left[\mathcal{U}_2^2+\mathcal{U}_4^2\right]^2\mathcal{U}_1^2R^2-\gamma^4R^4,\\
&\mathcal{V}_m^3=-2\left[\mathcal{U}_2R+\mathcal{U}_1\gamma\sin\theta\right]\gamma^{-4}R^{-3}, && \mathcal{V}_m^4=\left[\mathcal{U}_2^2+\mathcal{U}_4^2\right]^{-2}\mathcal{U}_1^{-2}R^{-2}-\gamma^{-4}R^{-4},\\
&\mathcal{V}_m^5=\left[\mathcal{U}_2^2+\mathcal{U}_4^2\right]\mathcal{U}_1^4\gamma^2-\gamma^4R^4, && \mathcal{V}_m^6=\left[\mathcal{U}_2^2+\mathcal{U}_4^2\right]^{-1}\mathcal{U}_1^{-4}\gamma^{-2}-\gamma^{-4}R^{-4},\\
&P=\frac{\widetilde{P}R_b}{\frac{\mu_1}{2}T}, && \mathfrak{M}=-\frac{\mu_2}{\mu_1}.
\end{aligned}\tag{46}$$

Non-dimensional principal Cauchy stresses in the θ and ϕ-directions are computed as

$$\sigma_{\theta\theta}=2\left[\frac{\lambda_1}{\lambda_2}-\frac{1}{\lambda_1^3\lambda_2^3}\right]\left[1+\mathfrak{M}\lambda_2^2\right],\quad \sigma_{\phi\phi}=2\left[\frac{\lambda_2}{\lambda_1}-\frac{1}{\lambda_1^3\lambda_2^3}\right]\left[1+\mathfrak{M}\lambda_1^2\right].\tag{47}$$

A.3 Coefficients for neo-Hookean model

The components of matrices in equation (14) for the neo-Hookean energy density are given by

$$\begin{aligned}
\mathcal{S}_{22} &= \left[\mathcal{U}_1 R^2\left[\mathcal{U}_2^2+\mathcal{U}_4^2\right]\left[\left[\mathcal{S}_n^1\right]\mathcal{U}_2^2+\left[\mathcal{S}_n^2\right]\mathcal{U}_4^2\right]\right]\lambda_1^6\lambda_2^2\gamma^4R^4,\\
\mathcal{S}_{24} &= \left[\mathcal{U}_1 R^2\left[\mathcal{U}_2^2+\mathcal{U}_4^2\right]\left[\left[\mathcal{S}_n^1\right]\mathcal{U}_2\mathcal{U}_4-\left[\mathcal{S}_n^2\right]\mathcal{U}_2\mathcal{U}_4\right]\right]\lambda_1^6\lambda_2^2\gamma^4R^4,\\
\mathcal{S}_{42} &= \mathcal{S}_{24},\\
\mathcal{S}_{44} &= \left[\mathcal{U}_1 R^2\left[\mathcal{U}_2^2+\mathcal{U}_4^2\right]\left[\left[\mathcal{S}_n^1\right]\mathcal{U}_4^2+\left[\mathcal{S}_n^2\right]\mathcal{U}_2^2\right]\right]\lambda_1^6\lambda_2^2\gamma^4R^4,
\end{aligned} \tag{48}$$

and

$$\begin{aligned}
\mathcal{V}_1 &= \left[\left[\mathcal{V}_n^2\right]\mathcal{U}_1\mathcal{U}_2\left[\mathcal{U}_2^2+\mathcal{U}_4^2\right]^2\gamma R\sin\theta+\left[\mathcal{V}_n^3\right]\left[\mathcal{U}_2^2+\mathcal{U}_4^2\right]^3R^2\right]\lambda_1^6\lambda_2^2\gamma^4R^4\\
&\quad-\left[\left[\mathcal{V}_n^1\right]\mathcal{U}_2\left[\mathcal{U}_2^2+\mathcal{U}_4^2\right]^2\right]\lambda_1^6\lambda_2^2\gamma^4R^4-\frac{P}{2}\mathcal{U}_1\mathcal{U}_4\left[\mathcal{U}_2^2+\mathcal{U}_4^2\right]^{\frac{3}{2}}\lambda_1^{11}\lambda_2^5\gamma^{10}R^{10},\\
\mathcal{V}_2 &= \left[\left[\mathcal{V}_n^2\right]\mathcal{U}_1\mathcal{U}_4\left[\mathcal{U}_2^2+\mathcal{U}_4^2\right]^2\gamma R\sin\theta\right]\lambda_1^6\lambda_2^2\gamma^4R^4-\left[\left[\mathcal{V}_n^1\right]\mathcal{U}_4\left[\mathcal{U}_2^2+\mathcal{U}_4^2\right]^2\right]\lambda_1^6\lambda_2^2\gamma^4R^4\\
&\quad+\frac{P}{2}\mathcal{U}_1\mathcal{U}_2\left[\mathcal{U}_2^2+\mathcal{U}_4^2\right]^{\frac{3}{2}}\lambda_1^{11}\lambda_2^5\gamma^{10}R^{10},
\end{aligned} \tag{49}$$

along with

$$\begin{aligned}
\mathcal{S}_n^1 &= \left[\mathcal{U}_2^2+\mathcal{U}_4^2\right]^2\mathcal{U}_1^2R^2+3\gamma^4R^4, & \mathcal{S}_n^2 &= \left[\mathcal{U}_2^2+\mathcal{U}_4^2\right]^2\mathcal{U}_1^2R^2-\gamma^4R^4,\\
\mathcal{V}_n^1 &= 2\left[\mathcal{U}_2R+\mathcal{U}_1\gamma\sin\theta\right]\gamma^4R^5, & \mathcal{V}_n^2 &= \left[\mathcal{U}_2^2+\mathcal{U}_4^2\right]^2\mathcal{U}_1^2R^2-\gamma^4R^4,\\
\mathcal{V}_n^3 &= \left[\mathcal{U}_2^2+\mathcal{U}_4^2\right]\mathcal{U}_1^4\gamma^2-\gamma^4R^4, & & \\
P &= \frac{\widetilde{P}R_b}{\frac{\mu_1}{2}T}. & &
\end{aligned} \tag{50}$$

Non-dimensional principal Cauchy stresses in the θ and ϕ-directions are computed as

$$\sigma_{\theta\theta}=2\left[\frac{\lambda_1}{\lambda_2}-\frac{1}{\lambda_1^3\lambda_2^3}\right],\quad \sigma_{\phi\phi}=2\left[\frac{\lambda_2}{\lambda_1}-\frac{1}{\lambda_1^3\lambda_2^3}\right]. \tag{51}$$

A.4 Matrix coefficients for wrinkled region

In the wrinkled region, using the relaxed energy density obtained by substituting $\lambda_2 = 1/\sqrt{\lambda_1}$, we find that the terms $S_{22}, S_{24}, S_{42}, S_{44}, \mathcal{V}_1, \mathcal{V}_2$ for each of the material models discussed above are modified as below.

For Ogden energy density, we get

$$
\begin{aligned}
\mathcal{S}_{22} &= \mu_1^* R\left[\varrho_\theta^2\left[\left[\alpha_1-1\right]\lambda_1^{\frac{3\alpha_1}{2}}+\left[\frac{\alpha_1}{2}+1\right]\right]+\eta_\theta^2\left[\lambda_1^{\frac{3\alpha_1}{2}}-1\right]\right]\lambda_1^{\frac{\alpha_2+\alpha_3}{2}+8}\\
&+\mu_2^* R\left[\varrho_\theta^2\left[\left[\alpha_2-1\right]\lambda_1^{\frac{3\alpha_2}{2}}+\left[\frac{\alpha_2}{2}+1\right]\right]+\eta_\theta^2\left[\lambda_1^{\frac{3\alpha_2}{2}}-1\right]\right]\lambda_1^{\frac{\alpha_1+\alpha_3}{2}+8}\\
&+\mu_3^* R\left[\varrho_\theta^2\left[\left[\alpha_3-1\right]\lambda_1^{\frac{3\alpha_3}{2}}+\left[\frac{\alpha_3}{2}+1\right]\right]+\eta_\theta^2\left[\lambda_1^{\frac{3\alpha_3}{2}}-1\right]\right]\lambda_1^{\frac{\alpha_1+\alpha_2}{2}+8},\\
\mathcal{S}_{24} &= \mu_1^* R\left[\varrho_\theta\eta_\theta\left[\left[\alpha_1-2\right]\lambda_1^{\frac{3\alpha_1}{2}}+\left[\frac{\alpha_1}{2}+2\right]\right]\right]\lambda_1^{\frac{\alpha_2+\alpha_3}{2}+8}\\
&+\mu_2^* R\left[\varrho_\theta\eta_\theta\left[\left[\alpha_2-2\right]\lambda_1^{\frac{3\alpha_2}{2}}+\left[\frac{\alpha_2}{2}+2\right]\right]\right]\lambda_1^{\frac{\alpha_1+\alpha_3}{2}+8}\\
&+\mu_3^* R\left[\varrho_\theta\eta_\theta\left[\left[\alpha_3-2\right]\lambda_1^{\frac{3\alpha_3}{2}}+\left[\frac{\alpha_3}{2}+2\right]\right]\right]\lambda_1^{\frac{\alpha_1+\alpha_2}{2}+8},\\
\mathcal{S}_{42} &= \mathcal{S}_{24},\\
\mathcal{S}_{44} &= \mu_1^* R\left[\eta_\theta^2\left[\left[\alpha_1-1\right]\lambda_1^{\frac{3\alpha_1}{2}}+\left[\frac{\alpha_1}{2}+1\right]\right]+\varrho_\theta^2\left[\lambda_1^{\frac{3\alpha_1}{2}}-1\right]\right]\lambda_1^{\frac{\alpha_2+\alpha_3}{2}+8}\\
&+\mu_2^* R\left[\eta_\theta^2\left[\left[\alpha_2-1\right]\lambda_1^{\frac{3\alpha_2}{2}}+\left[\frac{\alpha_2}{2}+1\right]\right]+\varrho_\theta^2\left[\lambda_1^{\frac{3\alpha_2}{2}}-1\right]\right]\lambda_1^{\frac{\alpha_1+\alpha_3}{2}+8}\\
&+\mu_3^* R\left[\eta_\theta^2\left[\left[\alpha_3-1\right]\lambda_1^{\frac{3\alpha_3}{2}}+\left[\frac{\alpha_3}{2}+1\right]\right]+\varrho_\theta^2\left[\lambda_1^{\frac{3\alpha_3}{2}}-1\right]\right]\lambda_1^{\frac{\alpha_1+\alpha_2}{2}+8},
\end{aligned}
\tag{52}
$$

along with

$$
\begin{aligned}
\mathcal{V}_1 &= \left[\mu_1^*\left[\lambda_1^{\frac{3\alpha_1}{2}}-1\right]\lambda_1^{\frac{\alpha_2+\alpha_3}{2}+10}+\mu_2^*\left[\lambda_1^{\frac{3\alpha_2}{2}}-1\right]\lambda_1^{\frac{\alpha_1+\alpha_3}{2}+10}+\mu_3^*\left[\lambda_1^{\frac{3\alpha_3}{2}}-1\right]\lambda_1^{\frac{\alpha_1+\alpha_2}{2}+10}\right]\gamma^3\mathcal{U}_2\sin\theta\\
&-\frac{\mu_1^*}{2}P\mathcal{U}_1\mathcal{U}_4\lambda_1^{\frac{\alpha_1+\alpha_2+\alpha_3}{2}+12}\gamma^3,\\
\mathcal{V}_2 &= \left[\mu_1^*\left[\lambda_1^{\frac{3\alpha_1}{2}}-1\right]\lambda_1^{\frac{\alpha_2+\alpha_3}{2}+10}+\mu_2^*\left[\lambda_1^{\frac{3\alpha_2}{2}}-1\right]\lambda_1^{\frac{\alpha_1+\alpha_3}{2}+10}+\mu_3^*\left[\lambda_1^{\frac{3\alpha_3}{2}}-1\right]\lambda_1^{\frac{\alpha_1+\alpha_2}{2}+10}\right]\gamma^3\mathcal{U}_4\sin\theta\\
&+\frac{\mu_1^*}{2}P\mathcal{U}_1\mathcal{U}_2\lambda_1^{\frac{\alpha_1+\alpha_2+\alpha_3}{2}+12}\gamma^3,\\
P &= \frac{2\widetilde{P}R_b}{\mu_1 T}.
\end{aligned}
\tag{53}
$$

For Mooney–Rivlin energy density, we get

$$
\begin{aligned}
\mathcal{S}_{22} &= R\left[\varrho_\theta^2\Big[\lambda_1^4+2\lambda_1+3\mathfrak{M}\Big]+\eta_\theta^2\Big[\lambda_1^4-\lambda_1+\mathfrak{M}\big[\lambda_1^3-1\big]\Big]\right],\\
\mathcal{S}_{24} &= R\left[\varrho_\theta\eta_\theta\Big[3\lambda_1+4\mathfrak{M}-\mathfrak{M}\lambda_1^3\Big]\right],\\
\mathcal{S}_{42} &= \mathcal{S}_{24},\\
\mathcal{S}_{44} &= R\left[\eta_\theta^2\Big[\lambda_1^4+2\lambda_1+3\mathfrak{M}\Big]+\varrho_\theta^2\Big[\lambda_1^4-\lambda_1+\mathfrak{M}\big[\lambda_1^3-1\big]\Big]\right],
\end{aligned}
\tag{54}
$$

along with

$$
\begin{aligned}
\mathcal{V}_1 &= \left[\lambda_1^4-\lambda_1+\mathfrak{M}\Big[\lambda_1^3-1\Big]\right]\gamma^3\lambda_1^2\mathcal{U}_2\sin\theta-\left[\left[\frac{P}{2}\right]\mathcal{U}_1\mathcal{U}_4\lambda_1^6\gamma^3\right],\\
\mathcal{V}_2 &= \left[\lambda_1^4-\lambda_1+\mathfrak{M}\Big[\lambda_1^3-1\Big]\right]\gamma^3\lambda_1^2\mathcal{U}_4\sin\theta+\left[\left[\frac{P}{2}\right]\mathcal{U}_1\mathcal{U}_2\lambda_1^6\gamma^3\right].
\end{aligned}
\tag{55}
$$

For neo-Hookean energy density, we get

$$
\begin{aligned}
&\mathcal{S}_{22} = R\left[\varrho_\theta^2\Big[\lambda_1^4+2\lambda_1\Big]+\eta_\theta^2\Big[\lambda_1^4-\lambda_1\Big]\right],\quad \mathcal{S}_{24} = R\left[\varrho_\theta\eta_\theta\Big[3\lambda_1\Big]\right],\\
&\mathcal{S}_{42} = \mathcal{S}_{24},\quad \mathcal{S}_{44} = R\left[\eta_\theta^2\Big[\lambda_1^4+2\lambda_1\Big]+\varrho_\theta^2\Big[\lambda_1^4-\lambda_1\Big]\right],
\end{aligned}
\tag{56}
$$

and

$$
\mathcal{V}_1 = \left[\lambda_1^4-\lambda_1\right]\gamma^3\lambda_1^2\mathcal{U}_2\sin\theta-\left[\left[\frac{P}{2}\right]\mathcal{U}_1\mathcal{U}_4\lambda_1^6\gamma^3\right], \tag{57}
$$

$$
\mathcal{V}_2 = \left[\lambda_1^4-\lambda_1\right]\gamma^3\lambda_1^2\mathcal{U}_4\sin\theta+\left[\left[\frac{P}{2}\right]\mathcal{U}_1\mathcal{U}_2\lambda_1^6\gamma^3\right]. \tag{58}
$$

References

Barsotti R. "Approximated solutions for axisymmetric wrinkled inflated membranes". *Journal of Applied Mechanics*, 82(11):111007 (2015)

Başar Y. and Itskov M. "Finite element formulation of the Ogden material model with application to rubber-like shells". *International Journal for Numerical Methods in Engineering*, 42(7):1279–1305 (1998)

Benedict R., Wineman A., and Yang W.H. "The determination of limiting pressure in simultaneous elongation and inflation of nonlinear elastic tubes". *International Journal of Solids and Structures*, 15(3):241 – 249 (1979)

Bonadies M. "Asymptotic behaviour of inflated toroidal elastic membranes". *Rendiconti del Seminario Matematico Università e Politecnico di Torino*, 45(3):63–74 (1987)

Budiansky B. "Theory of buckling and post-buckling behavior of elastic structures". volume 14 of *Advances in Applied Mechanics*, pages 1–65. Elsevier (1974)

Carroll M. "Pressure maximum behavior in inflation of incompressible elastic hollow spheres and cylinders". *Quarterly of Applied Mathematics*, 45(1):141–154 (1987)

Clark R.A. "On the theory of thin elastic toroidal shells". *Journal of Mathematics and Physics*, 29(1-4):146–178 (1950)

Dreyer W., Müller I., and Strehlow P. "A study of equilibria of interconnected balloons". *The Quarterly Journal of Mechanics and Applied Mathematics*, 35(3):419–440 (1982)

Epstein M. "On the wrinkling of anisotropic elastic membranes". *Journal of Elasticity*, 55(2):99–109 (1999)

Gruttmann F. and Taylor R.L. "Theory and finite element formulation of rubberlike membrane shells using principal stretches". *International Journal for Numerical Methods in Engineering*, 35(5):1111–1126 (1992)

Harold M.E. and Grenville P.A. "Load transfer via a wrinkled membrane". *Proceedings of the Royal Society of London. A. Mathematical and Physical Sciences*, 316(1525):269–289 (1970)

Haughton D. and McKay B. "Wrinkling of annular discs subjected to radial displacements". *International Journal of Engineering Science*, 33(3):335–350 (1995)

Hill J.M. "The finite inflation of a thick-walled elastic torus". *The Quarterly Journal of Mechanics and Applied Mathematics*, 33(4):471–490 (1980)

Holzapfel G.A. *Nonlinear Solid Mechanics: A Continuum Approach for Engineering*. Wiley (2000)

Holzapfel G.A., Eberlein R., Wriggers P., and Weizsäcker H.W. "A new axisymmetrical membrane element for anisotropic, finite strain analysis of arteries". *Communications in Numerical Methods in Engineering*, 12(8):507–517 (1996)

Horný L., Žitný R., Chlup H., and Hana M. "Identification of the material parameters of an aortic wall". *Bulletin of Applied Mechanics* (2007)

Humphrey J.D. "Computer methods in membrane biomechanics". *Computer Methods in Biomechanics and Biomedical Engineering*, 1(3):171–210 (1998)

Jenkins C.H., Haugen F., and Spicher W.H. "Experimental measurement of wrinkling in membranes undergoing planar deformation". *Experimental Mechanics*, 38(2):147–152 (1998)

Jordan P.F. "Stresses and deformations of the thin-walled pressurized torus". *Journal of the Aerospace Sciences*, 29(2):213–225 (1962)

Kanner L.M. and Horgan C.O. "Elastic instabilities for strain-stiffening rubber-like spherical and cylindrical thin shells under inflation". *International Journal of Non-Linear Mechanics*, 42(2):204–215 (2007)

Khayat R., Derdorri A., and Garcia-Réjon A. "Inflation of an elastic cylindrical membrane: non-linear deformation and instability". *International Journal of Solids and Structures*, 29(1):69–87 (1992)

Koiter W.T. *The Stability of Elastic Equilibrium*. Ph.D. thesis, Delft University of Technology (1945)

Kydoniefs A. and Spencer A. "The finite inflation of an elastic torus". *International Journal of Engineering Science*, 3(2):173–195 (1965)

Kydoniefs A. and Spencer A. "The finite inflation of an elastic toroidal membrane of circular cross section". *International Journal of Engineering Science*, 5(4):367–391 (1967)

Li X. and Steigmann D. "Finite deformation of a pressurized toroidal membrane". *International Journal of Non-Linear Mechanics*, 30(4):583–595 (1995a)

Li X. and Steigmann D. "Point loads on a hemispherical elastic membrane". *International Journal of Non-Linear Mechanics*, 30(4):569–581 (1995b)

Liepins A. and Sanders J.L. "Toroidal membrane under internal pressure". *The American Institute of Aeronautics and Astronautics Journal*, 1(9):2105–2110 (1963)

Mansfield E.H. "Gravity-induced wrinkle lines in vertical membranes". *Proceedings of the Royal Society A: Mathematical, Physical and Engineering Sciences*, 375(1762):307–325 (1981)

Müller I. and Struchtrup H. "Inflating a rubber balloon". *Mathematics and Mechanics of Solids*, 7(5):569–577 (2002)

Nayyar V., Ravi-Chandar K., and Huang R. "Stretch-induced stress patterns and wrinkles in hyperelastic thin sheets". *International Journal of Solids and Structures*, 48(25-26):3471–3483 (2011)

Ogden R.W. "Large deformation isotropic elasticity - on the correlation of theory and experiment for incompressible rubberlike solids". *Proceedings of the Royal Society A: Mathematical, Physical and Engineering Sciences*, 326(1567):565–584 (1972)

Papargyri-Beskou S. "Finite-element analysis of an axisymmetric, thin-walled, nonlinear elastic pressurized torus". *Acta Mechanica*, 178(1-2):1–22 (2005)

Papargyri-Pegiou S. "Stability of the axisymmetric analytical and numerical solutions in a thin-walled pressurized torus of compressible nonlinear elastic material". *International Journal of Engineering Science*, 33(7):1005–1025 (1995)

Papargyri-Pegiou S. and Stavrakakis E. "Axisymmetric numerical solutions of a thin-walled pressurized torus of incompressible nonlinear elastic materials". *Computers & Structures*, 77(6):747–757 (2000)

Patil A., Nordmark A., and Eriksson A. "Wrinkling of cylindrical membranes with non-uniform thickness". *European Journal of Mechanics - A/Solids*, 54:1–10 (2015)

Pipkin A.C. "The relaxed energy density for isotropic elastic membranes". *IMA Journal of Applied Mathematics*, 36(1):85–99 (1986)

Reddy N.H. and Saxena P. "Limit points in the free inflation of a magnetoelastic toroidal membrane". *International Journal of Non-Linear Mechanics*, 95:248–263 (2017)

Reddy N.H. and Saxena P. "Instabilities in the axisymmetric magnetoelastic deformation of a cylindrical membrane". *International Journal of Solids and Structures*, 136-137:203–219 (2018)

Roxburgh D.G. "Inflation of nonlinearly deformed annular elastic membranes". *International Journal of Solids and Structures*, 32(14):2041 – 2052 (1995)

Roychowdhury S. and DasGupta A. "Inflating a flat toroidal membrane". *International Journal of Solids and Structures*, 67-68:182–191 (2015)

Saxena P., Reddy N.H., and Pradhan S.P. "Magnetoelastic deformation of a circular membrane: wrinkling and limit point instabilities". *International Journal of Non-Linear Mechanics*, 116:250–261 (2019)

Steigmann D.J. "Tension-field theory". *Proceedings of the Royal Society A: Mathematical, Physical and Engineering Sciences*, 429(1876):141–173 (1990)

Steigmann D.J. "Puncturing a thin elastic sheet". *International Journal of Non-Linear Mechanics*, 40(2-3):255 – 270 (2005)

Stein M. and Hedgepeth J.M. *Analysis of partly wrinkled membranes.* National Aeronautics and Space Administration Technical Note D-813 (1961)

Szyszkowski W. and Glockner P. "Spherical membranes subjected to vertical concentrated loads: an experimental study". *Engineering Structures*, 9(3):183 – 192 (1987)

Tamadapu G. and DasGupta A. "In-plane surface modes of an elastic toroidal membrane". *International Journal of Engineering Science*, 60:25–36 (2012)

Tamadapu G. and DasGupta A. "Effect of curvature and anisotropy on the finite inflation of a hyperelastic toroidal membrane". *European Journal of Mechanics - A/Solids*, 46:106–114 (2014)

Tamadapu G., Dhavale N.N., and DasGupta A. "Geometrical feature of the scaling behavior of the limit-point pressure of inflated hyperelastic membranes". *Physical Review E*, 88(5):053201 (2013)

Wang F., Yuan C., Lu T., and Wang T.J. "Anomalous bulging behaviors of a dielectric elastomer balloon under internal pressure and electric actuation". *Journal of the Mechanics and Physics of Solids*, 102(February):1–16 (2017)

Wong W. and Pellegrino S. "Wrinkled membranes II: analytical models". *Journal of Mechanics of Materials and Structures*, 1(1):27–61 (2006)

Wriggers P. and Taylor R.L. "A fully non-linear axisymmetrical membrane element for rubber-like materials". *Engineering Computations*, 7(4):303–310 (1990)

Wu C.H. "The Wrinkled axisymmetric air bags made of inextensible membrane". *Journal of Applied Mechanics*, 41(4):963–968 (1974)

Wu C.H. "Nonlinear wrinkling of nonlinear membranes of revolution". *Journal of Applied Mechanics*, 45(3):533–538 (1978)

Wu C.H. and Canfield T.R. "Wrinkling in finite plane-stress theory". *Quarterly of Applied Mathematics*, 39(2):179–199 (1981)

Xin-chun S. and Chang-jun C. "Instability of toroidal membrane with large tensile deformation". *Applied Mathematics and Mechanics*, 12(6):557–564 (1991)

Yang W.H. and Feng W.W. "On axisymmetrical deformations of nonlinear membranes". *Journal of Applied Mechanics*, 37(4):1002–1011 (1970)

Zak M. "Statics of wrinkling films". *Journal of Elasticity*, 12(1):51–63 (1982)